HHS Public Access

Author manuscript

Genes Brain Behav. Author manuscript; available in PMC 2016 November 08.

Published in final edited form as:

Genes Brain Behav. 2015 November ; 14(8): 591–606. doi:10.1111/gbb.12259.

Systems genetic analysis of hippocampal neuroanatomy and spatial learning in mice

Anna Delprato[1,2,3], **Brice Bonheur**[1,2], **Marie-Paule Algéo**[1,2], **Philippe Rosay**[1,2], **Lu Lu**[4], **Robert W. Williams**[4], and **Wim E. Crusio**[1,2]

[1]University of Bordeaux, Institut de Neurosciences Cognitives et Intégratives d'Aquitaine, UMR 5287, Bat B2 - Allée Geoffroy St. Hilaire, CS 50023, 33615 Pessac cedex, France

[2]CNRS, Institut de Neurosciences Cognitives et Intégratives d'Aquitaine, UMR 5287, Pessac cedex, France

[3]BioScience Project, Wakefield, MA 01880, USA

[4]Department of Genetics, Genomics and Informatics, University of Tennessee Health Sciences Center, Memphis, TN 38163, USA

Abstract

Variation in hippocampal neuroanatomy correlates well with spatial learning ability in mice. Here we have studied both hippocampal neuroanatomy and behavior in 53 isogenic BXD recombinant strains derived from C57BL/6J and DBA/2J parents. A combination of experimental, neuroinformatic, and systems genetics methods were used to test the genetic bases of variation and covariation among traits. Data were collected on seven hippocampal subregions in CA3 and CA4 after testing spatial memory in an 8-arm radial maze task.

Quantitative trait loci (QTLs) were identified for hippocampal structure, including the areas of the intra- and infrapyramidal mossy fibers, stratum radiatum, and stratum pyramidale, and for a spatial learning parameter, error rate. We identified multiple loci and gene variants linked to either structural differences or behavior. *Gpc4* and *Tenm2* are strong candidate genes that may modulate intra- and infrapyramidal mossy fiber areas. Analysis of gene-expression networks and trait correlations highlight several processes influencing morphometrical variation and spatial learning.

Keywords

Hippocampus; spatial learning; recombinant inbred mice; complex traits; quantitative trait loci; systems genetics; radial maze; hippocampal morphometry

INTRODUCTION

Spatial navigation is a critical hippocampus-dependent skill (O'keefe & Nadel, 1978). Lesion studies have correlated damage to the hippocampus with impaired navigation ability (Chozick, 1983) and hippocampal volume and its fine structure covaries with performance

Correspondence to: Wim E. Crusio.

on navigational tasks in several bird and rodent species (Sherry *et al.*, 1992, Shettleworth, 1993). The wide individual variation in spatial learning and memory abilities among humans is also linked to differences in hippocampal size and morphology (Maguire *et al.*, 2003). One task to test spatial learning in rodents is the radial maze (Olton & Samuelson, 1976). Learning capability in this test is heritable and strongly strain-dependent. Strains such as C57BL/6 are fast learners while strains such as DBA/2 are slow learners (Crusio & Schwegler, 2005, Crusio *et al.*, 1987).

Similarly, large variation in the size of hippocampal fields (hilus, suprapyamidal and intra- and infrapyramidal mossy fibers, and the strata pyramidale, oriens, radiatum, and lacunosum-moleculare; Fig. 1) has been found in mice (Crusio *et al.*, 1986, Crusio & Schwegler, 2005). One projection in particular is highly variable among strains: the intra- and infrapyramidal mossy fiber (IIPMF) terminal field (Barber *et al.*, 1974), with a heritability of about 50% (Crusio *et al.*, 1986). The IIPMF projection is made up of axons of the dentate granular cells that project onto the pyramidal cells in CA3 (Andersen *et al.*, 2007). Large IIPMF projections are usually associated with good spatial learning abilities (Crusio & Schwegler, 2005). Manipulating this projection by means of inducing early postnatal hyperthyroidism results in larger IIPMF and improved learning in radial maze tasks (Crusio & Schwegler, 1991, Schwegler *et al.*, 1991), strongly suggesting a causal relation. To further understand the genetic basis of this behavioral and neuroanatomical variation and covariation, we exploited the large family of BXD recombinant inbred strains (Peirce *et al.*, 2004), to map QTLs linked to these traits. Although some previous studies to dissect the genetic architecture of hippocampal neuroanatomical variation were carried out (Lassalle *et al.*, 1999, Lu *et al.*, 2001, Peirce *et al.*, 2003), an analysis of radial-maze learning was not yet available.

The BXD strains are well suited for QTL analysis. They were derived from the C57BL/6J (B) and DBA/2J (D) parental strains. Both parental lines have been sequenced and differ at ~5.5 million loci—mainly single nucleotide polymorphisms (SNPs) and indels (Wang *et al.*, 2010, submitted). All genotypes, extensive phenome data, and many large expression data sets are publicly available at www.genenetwork.org.

QTL-mapping is a statistical method used to map chromosomal intervals (loci) that contribute to heritable variance in phenotypes. The method simply compares the inheritance of allelic variants (B or D genotypes in our case) with differences in phenotypes. A QTL will generally cover a region that includes 10 to 100 genes, and these positional candidates can then be ranked roughly on the basis of criteria such as the types of DNA variants, patterns of mRNA expression, data from complementary human genetic cohorts (GWAS and linkage) and relevant literature about gene effects on CNS structure and function. Given the correlations between spatial learning and hippocampal neuroanatomy, we hypothesized that at least some of the QTLs for these two categories would be shared.

MATERIALS AND METHODS

Subjects

Breeding pairs of 53 BXD strains were acquired from the University of Tennessee Health Center (Memphis, TN, USA) and the Neuro-Bsik consortium of the VU University Amsterdam (Amsterdam, The Netherlands). Breeding pairs of the parental strains, C57BL/6J (B) and DBA/2J (D), were obtained from Charles River (L'Arbresle, France). Our aim was to test 10 males and 10 females of each strain in the radial maze and to process half of these (i.e., 5 males and 5 females) for hippocampal morphometry. Because of logistical problems (for example, some strains not breeding well), we did not achieve this goal for all strains (see supplement). All animals were housed and bred in the SPF mouse facility of the University of Bordeaux (Pessac) in a climate-controlled breeding room (temperature: 21+/−1 °C, humidity: 55+/−10%, 12 hour light-dark cycle with lights on at 7 am). Food (Safe, type 113, sterilized) and water (softened, sterilized) were available *ad libitum.* Animals were housed 2–4 in classical (non-ventilated) clear plastic cages (162×406×176 mm, Tecniplast) filled with poplar wood shavings (Souralit). No other bedding or nesting material was provided.

Radial maze learning

Apparatus—The eight-arm radial maze used was similar to the one described previously (Supplementary Fig. 1; for a photograph, see Fig. 1 in Crusio & Schwegler, 2005). The central part measured 22 cm in diameter and the arms were 25 cm long, 6 cm high, and 6 cm wide. They were enclosed and made of transparent Plexiglas and the floor of the maze was colored gray. At the end of each arm some food pellets were deposited behind a perforated wall in order to prevent the mice from smelling the presence or absence of the food reward. A small fresh food pellet (approximately 10 mg) was placed in each arm behind a low barrier preventing the animal from seeing whether a specific arm was still baited or not. The maze was always oriented in space in the same way, but turned by 45° daily. Several extra-maze cues were provided close to the arms in a fixed configuration. A confinement procedure was used, consisting of transparent guillotine doors at the entrance of each arm. These doors were lowered and kept closed for 5s after the animal had returned to the central platform. This procedure is known to disrupt chaining responses and kinesthetic strategies in mice (Schwegler *et al.*, 1990). Two identical mazes were used, one to test female mice and one to test male mice.

We decided that the current experiment should have a power such that the correlation between RI strain means and a given genetic marker would reach 95% of the additive genetic correlation. The sample sizes necessary to obtain this goal were determined according to a method published earlier (Crusio, 2004). Briefly, heritabilities were estimated from data obtained in our previous studies (Schwegler *et al.*, 1990). For the size of the IIPMF, a value of around 0.50 was obtained, meaning that sample sizes of 5 animals per strain would be needed. For radial maze learning, heritability was estimated to be around 0.30. In order to have the correlation between strains reach 95% of the additive genetic correlation, a sample size of 10–11 animals per strain would therefore be required.

Procedure—All mice were tested in an open field for 20 min (not shown). Four days later the animals were tested in the radial maze as follows.

The maze was placed on the floor of a dedicated lighted procedure room in the animal facility. On the first day of testing, each mouse was weighed and subsequently subjected to a habituation session in which it was allowed to explore the maze freely for 10 min. Arm doors remained open, and no food was accessible in the maze. Mice were subsequently deprived of food, but not water, and were maintained at about 85% of their initial body weight throughout the experiment. The habituation trial was followed by five days of training with one trial per day, during which all eight arms contained a food reward. Animals were confined between arm visits for 5 seconds on the central platform by lowering the Plexiglas doors.

On the first 2 days of training, animals often entered an arm without eating the food reward. Therefore only results from the last 3 days of the training were included in the statistical analyses. Trials ended when an animal had found and eaten all eight rewards except on the first two days of training, where trials were stopped after a maximum of 30 minutes, even if an animal had not yet eaten all rewards. Animals were weighed daily. The experimenter was seated next to the maze, always in the same position. Arm visits were recorded using The Observer XT (Noldus, Wageningen, The Netherlands). An arm was considered visited if an animal entered it with all 4 paws. In between subjects, the maze was cleaned with water.

An error was counted if an animal entered an arm that had been visited before or without eating the reward (this happened only very rarely after the second day of training). Variables recorded were the total number of errors and the number of new arm entries during the first 8 arm visits. The maximum number of new entries is eight, whereas random choices will lead to an expected mean of 5.3 (Olton & Samuelson, 1976). In addition, the duration of each arm visit time was measured as a measure of activity.

Hippocampal histology and morphometry

Five days after the radial maze test, males were submitted to an aggression test. Three days later both males and females were perfused intra-cardiacally with sodium sulfide followed by glutaraldehyde and their brains removed for histology, weighed, and placed for 24 h in a postfixative solution of 3% glutaraldehyde and 20% sucrose. Subsequently, sections were developed for Timm's silver sulfide stain for heavy metals, which is associated with synaptic enzymes containing zinc (Danscher & Zimmer, 1978) and allows the visualization of the terminal fields of the hippocampal projections in the form of colored bands and patches. For morphometry, we selected the brains with the clearest histology/coloration, for a maximum of 5 males and 5 females per strain. We measured five horizontal 40-μm sections, taking every second one and starting at the midseptotemporal level, immediately after the disappearance of the septal pole. Both left and right hippocampi were measured. We used a microscope (Leica DM6000 B ×10) to make micrographs using an automated procedure to create composite photographs. The morphometrical analysis was performed using ImageJ (NIH v.1.48) with macros developed by one of us (BB). We determined the sizes of the three main mossy fiber (MF) terminal fields, namely, CA4 (hilus), suprapyramidal MF, and IIPMF, as well as of the stratum pyramidale, stratum oriens, stratum radiatum, and the

stratum lacunosum-moleculare (Fig. 1), and summed them over the five measured sections. Results for the subfields are expressed as percentages of the total hippocampus (CA3+CA4). This permitted an objective measurement, independently of the intensity of the coloration. We determined the sizes of the three main mossy fiber (MF) terminal fields, namely, CA4 (hilus), suprapyramidal MF, and IIPMF, as well as of the stratum pyramidale, stratum oriens, stratum radiatum, and the stratum lacunosum-moleculare (Fig. 1), and summed them over the five measured sections. Results for the subfields are expressed as percentages of the total hippocampus (CA3+CA4).

Statistical analysis

Strain and sex effects—All statistical analyses were performed with SAS 9.3 (SAS Institute Inc., Cary, NC, USA). To determine strain and sex effects, hippocampal morphometry and radial maze data were subjected to 2-way ANOVA with sex and strain as between-subjects and, if applicable, days of training as within subjects factors. Data are reported as means +/− SEM. Heritabilities were estimated according to the method of Hegmann and Possidente (1981). Briefly, h2 was defined as the ratio of the variance between strains divided by the sum of the within-strains and between-strains variances. These variance components were derived from the expected mean squares obtained with the SAS procedure GLM.

Bioinformatics—All of the genetic analyses were done in GeneNetwork which is an open source bioinformatics resource for systems genetics that exists as both a repository for genetic, genomic, and phenotypic data together with a suite of statistical programs for data analysis that includes mapping and evaluating QTLs, examining phenotype/genotype correlations, and building interaction networks.

QTL mapping—The QTL mapping module of GeneNetwork was used to identify QTLs for hippocampal morphometry and radial maze trait data. This module enables interval mapping, composite interval mapping, and a pairwise scan option to identify epistatic effects. QTL significance was assessed using the likelihood ratio statistic (LRS) obtained after 5000 permutations and 2000 bootstrap tests. QTLs were deemed significant if $P<0.05$ and suggestive if $P<0.63$, which yields, on average, one false positive per genome scan. Male and female data were analyzed separately because of possible interactions between strain and sex. Outliers were winsorized.

All genes located within significant QTL intervals were screened with the QTLminer component of GeneNetwork (Alberts & Schughart, 2010). QTLminer is a program that integrates information for all the genes present within a specific genomic region such as functional annotation, gene expression data, sequence polymorphisms, cis-regulation data, and KEGG pathway associations. Functional associations and gene ontology for candidate genes were further assessed using Gene (http://www.ncbi.nlm.nih.gov/gene), DAVID (http://david.abcc.ncifcrf.gov), Webgestalt (http://bioinfo.vanderbilt.edu/webgestalt/) and literature mining using PubMed (http://www.ncbi.nlm.nih.gov/pubmed). The percentage of the variance between means explained by a certain QTL was calculated as the square of the correlation between the strain means and the genetic marker with the highest LRS score

(note that to some extent this will be an overestimation, due to the "Beavis effect"; see Xu, 2003).

Correlation analyses—Radial maze and hippocampal trait data, for which significant and nearly significant QTLs were obtained, were correlated against an mRNA expression dataset (Affymetrix Hippocampus Consortium M430v2 MAS5, http://www.genenetwork.org/dbdoc/Hippocampus_M430_V2_PDNN_Sept05.html) and the behavioral phenotypes database in GeneNetwork. The top 200 correlates were considered for both mRNA expression and behavioral phenotypes data. Covariates were rank correlated using Spearman's rank correlation (Siegel, 1956). For covariates with a P-value ≤ 0.02 and the number of common strains ≥10, data were exported to Cytoscape for network construction and visualization.

3D modeling—The mouse GPC4 protein structure was modeled in normal mode with the Phyre2 server (http://www.sbg.bio.ic.ac.uk/phyre2/html/page.cgi?id=index) using the crystal structure of the GPC1 human homolog (pdb id: 4ACR chain B) as a template. The GPC4 structure was modeled with 100% confidence for 424 residues, representing 76% coverage.

RESULTS

Raw data

All data have been deposited in the GeneNetwork database and are publicly available (trait IDs male/female: hippocampal morphometry, IIPMF: 16307/17476; hilus: 17483/17477; suprapyramidal MF 17484/17478; stratum pyramidale: 17485/17479; stratum oriens: 17486/17480; stratum radiatum: 17487/17481; stratum lacunosum-moleculare: 17488/17482: weights, body weight 17489/17492; brain weight: 17490/17493; relative brain weight: 17491/17494; radial maze: errors day 3: 17495/17507; errors day 4: 17496/17508; errors day 5: 17497/17509; total errors: 17498/17510; new entries day 3: 17499/17511; new entries day 4: 17500/17512; new entries day 5: 17501/17513; new entries total: 17502/17514; arm visit time day 3: 17503/17515; arm visit time day 4: 17504/17516; arm visit time day 5: 17505/17517; total arm visit time: 17506/17518).

Body and brain weights

Data for initial body weight at the beginning of radial maze testing were available for 432 female (52 strains) and 444 male mice (53 strains). Of these, brain weights were available for 426 female (52 strains) and 434 male mice (53 strains), as well as for 10 males and 10 females for each of the parental strains. Two-way ANOVA indicated significant strain differences for body weight ($F_{54,805}$=13.36, P<0.001), brain weight ($F_{54,789}$=8.59, P<0.001) and relative brain weight ($F_{54,789}$=11.62, P<0.001; see Table S1). Significant sex differences were also observed for body weight ($F_{1,805}$=1023.08, P<0.001) and brain weight relative to body weight ($F_{1,789}$=983.09, P<0.001), but not for brain weight itself ($F_{1,789}$=0.50, ns). Significant strain-by-sex interactions were observed for body weight ($F_{53,805}$=2.56, P<0.001) and relative brain weight ($F_{53,789}$=2.26, P<0.001), but not for brain weight itself ($F_{53,789}$=1.20, ns). Strain distribution patterns and heritabilities are presented in Fig. S2. Heritabilities were rather high for both males and females and were similar for the different variables, with an average of 0.39 for males and 0.41 for females.

Radial-maze learning

For the spatial learning and navigation test, the performances of 914 mice were evaluated for their ability to learn a standard 8 arm radial maze (see Table S2). Data were obtained from 451 female (52 strains) and 463 male mice (53 strains), as well as for 10 males and 10 females for each of the parental strains. Overall, there was a normal learning curve with errors decreasing over days (Days: $F_{2,1602}$=20.43, p<0.0001) and new entries increasing (Days: $F_{2,1602}$=12.27, p<0.001; Fig. 2, Fig. S3 and S4).

Errors—Large differences were found between strains ($F_{53,801}$=2.30, p<0.001) and sexes ($F_{1,801}$=5.47, p<0.05), with females making more errors than males. There was no significant strain*sex interaction ($F_{53,801}$<1, ns). Not all strains learned at the same rate (Days*Strain: $F_{106,1602}$=1.35, P<0.05).

New entries—Here, too, large differences between strains were found ($F_{53,801}$=2.53, p<0.001), but sex*strain effects were not significant (F<1). Not all strains learned at the same rate (Days*Strain: $F_{106,1602}$=1.29, P<0.05).

Learning was also evaluated by testing whether the total new entries over days 3–5 deviated significantly from random (5.3, t-test). For 44 strains sufficient data were available for this analysis (see Tables S3–S6). About two-thirds of the strains learned. For twenty-six of these strains, this was the case for both males and females. There were 5 strains (BXD40, BXD81, BXD28, BXD80, and BXD43) in which only females learned and 6 strains (BXD97, DBA/2J, BXD16, BXD42, BXD70, and BXD27) in which only males learned.

Arm visit time—Time spent per arm visit decreased with training (Days:$F_{2,1602}$=35.15, P<0.001; Fig. 2). There were considerable differences between strains (Strain: $F_{53,801}$=3.71, p<0.001; Days*Strain: $F_{106,1602}$=1.69, P<0.001). Differences between males and females appeared in a strain dependent manner (Sex: $F_{1,801}$=1.67, ns; Sex*Strain: $F_{53,801}$=1.79, p<0.001).

Strain distribution patterns and heritabilities are presented in Fig. S3. Heritabilities were low for both males and females and were similar for the different variables, with an average of 0.10 for males and 0.11 for females.

Hippocampal morphometry

Data were obtained from 207 female (51 strains) and 215 male mice (53 strains), as well as for 5 males and 5 females for each of the parental strains (Table S1). A repeated-measures ANOVA of the left and right total sizes of the CA3+CA4 fields showed large differences between strains ($F_{52,342}$=3.03, P<0.001). However, no differences were found between sexes ($F_{1,342}$<1, ns) and there was no strain*sex interaction ($F_{52,342}$=1.03, ns). Left-right differences missed significance ($F_{1,342}$=3.12, P=0.08). However, they did not interact with any other factor (LR*Strain, LR*sex:, LR*strain*sex: F<1, ns). Therefore whatever left-right differences are present in these data, they were similar over strains or sexes. Therefore, all following analyses were performed on left-right mean values.

Significant strain differences ($p<0.001$) were observed for all 7 hippocampal traits measured (IIPMF: $F_{52,342}=8.61$, Hilus: $F_{52,342}=7.09$, suprapyramidal MF $F_{52,342}=4.59$, stratum pyramidale: $F_{52,342}=3.79$, stratum oriens: $F_{52,342}=2.86$, stratum radiatum: $F_{52,342}=6.70$, stratum lacunosum-moleculare: $F_{52,342}=3.12$; see Fig. S5 and Table S1). Significant sex differences ($p<0.001$) were observed for the stratum oriens ($F_{1,342}=10.95$), stratum radiatum ($F_{1,342}=11.51$), and stratum lacunosum-moleculare ($F_{1,342}=10.05$). Significant sex-by-strain interactions ($p<0.05$) were observed for the stratum lacunosum-moleculare ($F_{52,342}=1.46$, see Table S1). Heritabilities ranged from 0.04–0.46 with an average of 0.27 for males and for females from 0.16–0.45 with an average of 0.31. For both sexes, the lowest h^2 measure was obtained for the stratum oriens and the highest for the IIPMF. Strain distribution patterns and heritabilities are presented in Fig. S5.

Bi- and multivariate analyses

Moderate Spearman rank correlations were observed among morphometrical traits (Tables S7a and S7b). For females: stratum oriens correlated negatively with the hilus ($r_S=-0.53$), stratum pyramidale ($r_S=-0.54$) and stratum lacunosum-moleculare ($r_S=-0.50$). For males, negative correlations were also observed for the stratum oriens and hilus ($r_S=-0.63$). In addition, new entries correlated with errors (males: $r_S=-0.55$, females: $r_S=-0.41$). However, there were no significant correlations between hippocampal morphometry and spatial learning.

A multivariate factor analysis of hippocampal morphometry and radial maze learning was performed on strain means for the BXD and parental lines. Seven hippocampal morphometry variables and two learning variables produced two factors with an Eigenvalue >1 structure for both the male and female data sets (Table S8), which were subjected to an orthoblique Harris-Kaiser rotation.

For females, Factor 1 had 5 loadings ≥ |0.3|, which were all related to hippocampal morphometry. Factor 2 had 3 loadings ≥ |0.3|. Two of these were related to hippocampal morphometry (hilus and suprapyramidal MF) and one was associated with learning (new entries).

For males, Factor 1 had 7 loadings ≥ |0.3|. These were five related to hippocampal morphometry, plus the two learning variables. Hilus, stratum lacunosum molecular, suprapyramidal MF, and errors had positive loadings while the stratum oriens, stratum radiatum, and new entries had negative ones. Factor 2 had 4 loadings ≥ |0.3|. Two were related to morphometry, plus the two learning variables. The IIPMF, suprapyramidal MF, and new entries had positive loadings whereas errors had a negative one.

QTL mapping of individual variables

Significant QTLs were detected for three of the seven hippocampal morphometry traits: IIPMF, stratum pyramidale, and stratum radiatum (Figs. 3 and 4, Fig. S6, and Table 1). A QTL just shy of the threshold for significance was detected for the size of the hilus in males (Fig. S6). Finally, a significant QTL was mapped for radial maze error rate (Fig. 4 and Table 1). No significant QTLs were found for brain or body weight, new entries, or arm visit time (Fig. S7–S9). In general, strains that inherited the *B* haplotype at these loci had larger

IIPMF, stratum radiatum, and stratum pyramidale sizes and made fewer errors. Composite interval mapping controlling for each of the QTLs did not reveal any secondary QTLs. In addition, no significant pairwise epistatic interactions were found between these QTLs.

To identify candidate genes, the areas under the QTL peaks and shoulders that cross the suggestive threshold were screened. The selection criteria used here were based on criteria used in similar studies: (1) whether a gene is expressed in the relevant tissue (the hippocampus), (2) presence of SNPs within the candidate genes (3) the occurrence of missense or non-synonymous mutations or other DNA variants, and (4) the presence of cis acting expression QTLs (Alberts & Schughart, 2010).

Errors—For the radial maze learning parameter, total errors, a significant QTL peak (LRS=17.9) was identified in females on Chr 3 (Table 1 and Fig. 4), explaining 26% of the variance between strain means. The peak LRS was broad and occurred at 12.6–15.8 Mb. The support interval for the QTL ranged from 5–20 Mb and contained 82 genes. This initial gene list was filtered to three candidates, including carbonic anhydrase-2 (*Car2*), *RNA binding protein-like* (*Ralyl*), and *1810022K09Rik* (human *C8orf59*). *Car2* is a cytosolic zinc metalloenzyme that catalyzes the reversible hydration of CO_2 and, like other family members, regulates pH and fluid balance in different regions of the body (Lindskog, 1997). *Car2* may modulate neuronal signaling by enhancing bicarbonate-driven GABAergic excitation during intense $GABA_A$ receptor activation (Ruusuvuori *et al.*, 2013). *Ralyl* (*Raly-like recognition motif*) is an RNA-binding protein that plays a critical role in embryonic development (Ji *et al.*, 2003). There is currently minimal functional annotation for *1810022K09Rik/C8orf59*, but this gene is well expressed in mouse and human hippocampus (Gtex Consortium, 2015).

IIPMF—Two QTLs contributing to IIPMF size were identified on Chrs X (males) and 11 (males and females, Fig. S6). In males a significant peak (LRS=18.24) was observed at 48.1 Mb on Chr X, explaining 26% of the variance between strain means. The interval including shoulders and peak ranged from 45–60 Mb. In females a suggestive peak occurred at about the same chromosomal location. The initial list consisting of 107 candidate genes was narrowed down to a single gene that met all selection criteria: *Gpc4* is a member of the Glypican family of membrane associated proteins that interact with cell surface and extracellular matrix proteins (Filmus & Selleck, 2001). Glypicans play an important role in developmental morphogenesis and also in the regulation of Wnt and Hedgehog cell signaling pathways (Achouche *et al.*, 1992, Fico *et al.*, 2011, Filmus & Capurro, 2014, Sakane *et al.*, 2012, Serralbo & Marcelle, 2014). *Gpc4* KO mice indicate a functional role for this gene in synapse formation via the glutamate receptors where it facilitates clustering and receptivity (Allen *et al.*, 2012). While there is no direct structural information available for the GPC4 protein, a threaded model based on the crystal structure of human GPC1 indicates that the non synonymous mutation A537T occurs in a disordered loop region at the C-terminus (Fig. S10).

For Chr 11, a highly suggestive peak was observed at position 42.6 Mb (Fig. S6) for both males (LRS=15.2) and females (LRS=15.9), explaining 28% and 25% of the variance between strain means, respectively. The range, including the peak and shoulders spanned

34–43 Mb. This region of Chr 11 consisted of 25 genes which were narrowed to two candidates: *Tenm2* and *Gabrg2*. *Tenm2* encodes the teneurin 2 transmembrane glycoprotein which is expressed during pattern formation and morphogenesis (Rubin *et al.*, 1999, Zhou *et al.*, 2003). Teneurin-2 facilitates cell-cell contact, cell recognition, and cell adhesion (Rubin *et al.*, 1999). Relative to neuronal function, the teneurin protein family has a role in neuronal path finding and axon guidance (Kenzelmann *et al.*, 2008, Young & Leamey, 2009). The H243P amino acid substitution occurs in the N-terminal region which has been implicated in transcription factor activity (Bastias-Candia *et al.*, 2015, Nunes *et al.*, 2005) (Fig. S10).

Gabrg2 encodes the gamma 2 subunit of the gamma aminobutyric acid ($GABA_A$) receptor. Mutations in *Gabrg2* have been associated with epilepsy and febrile seizures (Hirose, 2014, Saghazadeh *et al.*, 2014). The non-synonymous mutation Ala to Thr occurs at amino acid position 49 at the N-terminus which is extracellular and outside of its known functional domains but may be part of a signaling motif. Due to its critical role in neuronal signaling, the *Gabrg2* gene cannot be excluded as a factor influencing IIPMF size. However, additional data supports *Tenm2* as the stronger candidate. This is based on sequence data obtained over 15-years ago from two inbred selection lines, SRH and SRL, which were derived from an F_2 cross between DBA/2 and C57BL/6 (Van Abeelen, 1970). Males were selected for high versus low rearing behavior in an open field and, for four generations, backcrossed to DBA/2 females. After this, the selection was continued combined with sib-mating. The resulting inbred selection lines were found to differ in the sizes of their IIPMF (Crusio *et al.*, 1989). These strains were genotyped (Worksheet S1) which showed that, as expected, they were highly similar to DBA/2, but some C57BL/6 derived material was present on Chrs 2, 3, 4, 6, 9, 11, 12, and 18. On Chr 11, the recombination interval was located at 0–40.25 Mb, partially overlapping with the highly suggestive QTL obtained in this study (34–43 Mb), narrowing down the region of interest to the interval between 34 and 40.25 Mb (with the region up till 36.9 Mb *B* haplotype-derived and the crossover point located somewhere between 36.9 Mb and 42.6 Mb). *Tenm2* lies squarely in the B6-derived region, but *Gabrg2* is rather close to the *D* haplotyê-derived region, supporting *Tenm2* as the more likely candidate. Unfortunately, the SRH/SRL lines are extinct so that it is not possible to investigate this interval in finer detail.

Stratum radiatum—A significant QTL was identified for the stratum radiatum in males (LRS=17.2) on Chr 2 at 16.2–17.8 Mb (Table 1 and Fig. 4), explaining 24% of the variance between strain means. The relevant interval ranged from 11–34 Mb and contained 353 genes. This list was reduced to 10 interesting candidates. Of these, four genes are related to neurological processes and pathologies: *Fbxw5* - Parkinson's disease (Ha *et al.*, 2014), *Armc3* - late onset Alzheimer's disease (Grupe *et al.*, 2006) and Asperger's syndrome (Steeb *et al.*, 2014), *Kcnt1* – epilepsy (Becchetti *et al.*, 2015), *Ptgds* – schizophrenia (Harrington *et al.*, 2006, Li *et al.*, 2008), Parkinson's disease, Creutzfeldt-Jakob disease, and multiple sclerosis (Harrington *et al.*, 2006).

Stratum pyramidale—A significant QTL was identified for the stratum pyramidale in females on Chr 11 with peaks at 26.8 and 28.4 Mb (LRS 23.4 and 21.6, respectively; Table 1 and Fig. 4), explaining 26% of the variance between strain means. The interval considered

ranged from 30–60 Mb and contained 365 genes which narrowed to 20 possible candidates. There was no functional information available for 2 (1810073G14Rik and 9530068E07Rik). Of the other 18, six genes can be connected to neurological processes and/or pathologies: *Agxt2l2*: Autism spectrum disorder and neurotransmission (Cusco *et al.*, 2009); *Hint1*: nicotine dependence (Jackson *et al.*, 2012), mu-opioid receptor binding (Garzon *et al.*, 2015, Rodriguez-Munoz *et al.*, 2015), depression (Martins-De-Souza *et al.*, 2012), and schizophrenia (Vawter *et al.*, 2002), *Gemin5*: motor neuron survival (Battle *et al.*, 2006, Gubitz *et al.*, 2002), Slc22a4: neuronal differentiation (Nakamichi *et al.*, 2012) and *Tenm2 and Gabrg2* which have already been described in the previous section on the IIPMF. It should be noted that the peaks on Chr 11 for the IIPMF and stratum pyramidale overlap.

Hilus—An almost significant QTL peak was identified for the size of the hilus in males (LRS=16.258) on Chr13 at 107.8 Mb (Fig. S6). The interval ranged from 106.5–108.5 Mb and contained 9 genes. One of these genes, *Ipo11*, met the selection criteria. The protein product, Importin 11, belongs to a family of transport receptor proteins that facilitate nuclear/cytoplasmic transport of protein and RNA cargo (Wagstaff & Jans, 2009). Importins also shuttle transcription factors like CREB that are associated with memory and synaptic plasticity (Forwood *et al.*, 2001).

Just after the major peak, the curve plateaus before dropping to baseline. When this region is included in the analysis, the interval is extended from 106–112 Mb and there are 2 more genes that meet the selection criteria: *Pde4d* and *Rab3c*. *Pde4d* controls intracellular cyclic AMP signaling. A KO mouse for *Pde4d* demonstrated enhanced spatial memory formation and hippocampal neurogenesis (Rutten *et al.*, 2008). Rab3c is a small GTPase that has well defined roles in synaptic vesicle transport, neurotransmitter release, and Ca^{2+} mediated exocytosis (Schluter *et al.*, 2004). Both of these genes along with *Ipo11*, are associated with neuronal processes like hippocampal-dependent memory formation and learning, making it impossible to discern a best candidate based on functional association (Li *et al.*, 2011, Rutten *et al.*, 2008, Schluter *et al.*, 2006, Tsetsenis *et al.*, 2011).

Suggestive QTLs shared between males and females—Suggestive QTL peaks common between males and females occurred for the stratum laconosum-moleculare (Chr 3), stratum oriens (Chr 5), suprapyramidal MF (Chr 1 and Chr 10), stratum radiatum (Chr 2), and IIPMF (Chr 8, Fig. S7). For the learning traits and for brain and body weight no common QTLs were observed between males and females (Fig. S8 and S9).

QTL mapping of combined traits

Factor analysis of the morphometry and learning variables produced a 2-factor solution for both males and females (Table S7). The factor scores were used to identify QTL loci. No significant QTLs were found for any of the factors (Fig. S11). In males, suggestive QTLs were obtained for factor 1 on Chrs 3, 5, and 10. For factor 2 suggestive QTLs were identified on Chr 2 and Chr 11. In females, no suggestive QTLs were found for factor 1 and borderline suggestive QTLs for factor 2 on Chrs 15 and 19.

IIPMF gene interaction analysis

For the traits in which significant QTLs were obtained, the data were further used to identify and explore gene interactions with hippocampal mRNA expression datasets. The correlates were visualized as interaction network graphs where the nodes represent genes and the edges represent the correlation value (Fig. 5 and Worksheet S2). Of all the graphs representing the traits under study, the IIPMF graph is the only one that has interconnectivity between genes. It also has the most edges and the highest correlation values of all traits, ranging from |0.6| to |0.85|. For the other traits, all correlations are smaller than |0.6| with one exception (hilus size and gene id *4930579G24*).

For the IIPMF morphometry data, the network contained 26 nodes and 33 edges. Of these correlates, 17 were positive and 16 were negative. The graph contains 2 clusters that are marked by interconnectivity and high correlation values (Fig. 5). One of the clusters contains 5 genes: *Ncam1*, *Ssbp3*, *2900034C19*, *Rps12*, and *Ndufs8*, and has 6 edges. *Ncam1* is involved in neural cell adhesion, growth, and migration (Basu *et al.*, in press). *Ssbp3* has been shown to regulate head morphogenesis in mouse embryos and is involved in midbrain and hindbrain boundary formation (Enkhmandakh *et al.*, 2006, Nishioka *et al.*, 2005). There is no functional information available for *2900034C19* but in the cluster it correlates positively with *Cugbp1* whose function is RNA binding and regulation of multicellular organism growth (Lambert *et al.*, 2014, Lu *et al.*, 2015). Overexpression of *Cugbp1* in a transgenic fly model of Fragile X suppressed the neurodegenerative associated tremor/ataxia associated with the disease (Sofola *et al.*, 2007).

Rps12 codes for a subunit of the 40S ribosome. An RNAi study showed a role for *Rps12* in regulating migration and proliferation in gastric cancer cells (Chen *et al.*, 2013, Herault *et al.*, 1991). Ndufs8 (NADH dehydrogenase (ubiquinone) Fe-S protein 8) is a subunit of the mitochondrial complex 1, the largest multi-enzyme complex (45 subunits) of the mitochondrial respiratory chain that transfers electrons from NADH2 to ubiquinone. Mitochondria complex I mutations have been found in Leigh syndrome and several other neurological disorders such as Schizophrenia, Parkinson's, and Alzheimer's diseases (Akarsu *et al.*, 2014, Mancuso *et al.*, 2009, Procaccio & Wallace, 2004, Song & Cortopassi, 2015). Correlations between *Ncam1/Ndufs8* and *Ncam1/Rps12* are negative, whereas all others are positive (*Rps12/Ndufs8*, *Ncam1/2900034C19*, *Ncam1/Ssbp3*, *Ssbp3/Rps12*).

The second cluster in the IIPMF network has 6 genes (*Tenm2, Gabra1, Pttg1, Prorsd1, Rhbdf1*, *Rtn4*) and 7 edges and is centered around *Tenm2*. *Gabra1/Tenm2, Tenm2/Ptgg1, Prorsd1/Rhbdf1*, and *Rhbdf1/Rtn4* are negatively correlated whereas *Gabra1/Pttg1, Tenm2/Prorsd1*, and *Tenm2/Rhbdf1* are positively correlated. As described in detail in an earlier section, Tenm2/Teneurin-2 is a transmembrane protein involved in cell adhesion and migration. For the other covariates Gabra1 is a receptor ligated-gated ion channel, and *Pttg1/Securin* is involved in cell migration and has been implicated in many types of cancers (Castilla *et al.*, 2014, Kash *et al.*, 2003, Yoon *et al.*, 2012). It is an inhibitor of separase, which is a protease required for the separation of sister chromatids in mitosis and meiosis (Tong *et al.*, 2008, Waizenegger *et al.*, 2002). Prorsd1 is uncharacterized but it contains a YbaK domain that is associated with proteins involved in tRNA editing activity, Rtn4 is

associated with neurite outgrowth and inhibition of neuronal plasticity, and Rhbdf1 with apoptosis and autophagy (Chong *et al.*, 2012, Raiker *et al.*, 2010, Yan *et al.*, 2008).

Network merge

The network graphs were merged to potentially identify common genes that may affect hippocampal morphometry. Only the IIPMF and stratum pyramidale graphs intersected (Fig. 6). The merged network contains 39 genes and 47 edges. The graphs connect through two genes, *Bcl2l11* which negatively covaries and *Ndufs8* which correlates positively. *Bcl2l11* acts as an apoptotic activator and its expression can be induced by nerve growth factor (NGF), as well as by the forkhead transcription factor, FKHR-L1, suggesting a role for this gene in neuronal and lymphocyte apoptosis (Dai & Grant, 2015, Putcha *et al.*, 2001, Sohn *et al.*, 2003, Yin *et al.*, 2006). Ndufs8 is a subunit of the MCI complex and is one of the cluster proteins described above. Ndufs8 connects directly to Rps12 and Ncam1. There is no physical evidence for direct protein-protein interactions but Bcl2l11 and Ndufs8 appear in a common KEGG pathway map (#04932 non-alcoholic fatty liver disease). There are no KEGG pathway maps for any of the other genes/proteins in the clusters at this time.

Functional enrichment of the genes indicates that most are involved in cell adhesion, growth, and migration (Fig. 7). For the other graphs there was no concentrated enrichment. Graphs and functional categories are provided in Fig. S13).

Trait correlation analysis

The trait data for which significant QTLs were obtained were used to identify covariates within the GeneNetwork traits database. For each trait, the first 200 correlates were filtered according to whether Spearman's rho was significant at $P<0.01$ and based on at least 10 common BXD strains (see Worksheet S3). The strongest correlations ($P\geq0.7$) are related to IIPMF, stratum pyramidale, and stratum radiatum sizes. They are shown as a network graph together with the correlations with radial maze errors in Fig. 8.

For the IIPMF in males, the strongest positive correlates are iron levels in medial prefrontal cortex (trait ID 10240), Dopamine receptor 2 membrane binding in the dorsal striatum (10264), and exploratory activity in response to cocaine (10312). The strongest negative covariates are iron levels in the liver (10248), field potentials in L2/3 of the primary whisker motor cortex (17154), HSV-1 virulence, (trait id 16185), thymus to body size ratio (10463), open arm entries on an elevated plus maze (10909) and prepulse inhibition in a Huntington model (13495).

The strongest positive covariates for the stratum radiatum in males are seizure susceptibility (trait ID 10451), open-field defecation in a Huntington model (13442), ethanol consumption (13578), and preference for a grid textured floor (10101). The strongest negative covariates are resistance to lymphoma tumors (10716), copper levels in dorsal striatum and ventral midbrain (10734, 10728), and field oscillations in L2/3 of the primary whisker motor cortex (17201).

For the stratum pyramidale in females, the strongest positive covariates are body weight and left hemisphere brain weight in a Huntington model (trait IDs 13518, 13512), body

temperature after ethanol administration (10510, 10521), open field center time after cocaine administration (10329), iron levels in ventral midbrain (10245), locomotor activity (11633), and nose pokes in a holeboard after cocaine administration (10312). The strongest negative covariates are HSV-1, serum neutralizing antibody titer and virulence (16305).

The strongest positive correlates for errors in females are brain weight and soluble/aggregate protein in a Huntington model (trait IDs 16188, 14787, 16190), oscillations with the respiratory rhythm and coherence in L2/3 of the primary whisker motor (17085, 17191), deep mesencephalic nuclei volume (trait id 10936), blood creatinine concentration (12846), and time in the center of an elevated plus maze (10905, 10896). The strongest negative correlates are Rant cytokine activity in draining lymph nodes post *Leishmania major* infection (12726), total distance run in an open field after cocaine administration (10317), median survival after bacterial infection (14833, 14834), and zinc levels in the medial prefrontal cortex (10725).

DISCUSSION

Learning performance in a radial maze, a hippocampus-dependent task (O'keefe & Nadel, 1978), shows strong, heritable variation between different inbred strains, as does hippocampal neuroanatomy. In addition, previous work has shown that learning performance and hippocampal morphometry are strongly correlated. Specifically, mice with large intra- and infrapyramidal terminal fields (IIPMF) generally make fewer errors in this task and this correlation appears to be mainly genetic (Crusio & Schwegler, 2005). In addition, increasing the size of the IIPMF by inducing early postnatal hyperthyroidy predictably improves performance in the radial maze (Crusio & Schwegler, 1991, Schwegler *et al.*, 1991), making it highly likely that this correlation is causal. No systematic correlations between learning and other hippocampal fields have been reported. We therefore used the BXD cohort and a forward genetics approach to identify QTLs and novel regulators underlying these heritable differences in spatial learning in a radial maze and hippocampal morphometry, hypothesizing that part of the genetic variation in behavior and neuroanatomy would be shared. Our strategy included testing a large number of BXD genotype (>>30, cf.: Wang *et al.*, 2014) and a large within strain sample size to increase strain mean accuracy and to increase the likelihood of QTL detection and mapping.

QTL mapping of individual variables

No significant QTLs were identified for body or brain weight, probably indicating a highly-polygenic mode of inheritance for these characteristics, with each individual gene's contribution below the detection threshold of this study. Suggestive QTLs were found on chromosomes 8 and 17 for relative brain weight in females. Others studies have reported significant loci on chromosomes 11 and 19 (e.g., Hager *et al.*, 2012; trait IDs 11016, 12661).

For learning, we identified a significant QTL on Chr 3 for the variable "number of errors days 3–5". Further analysis identified three candidate genes. Of those, *Car2* is the only gene at this time that can be associated with neuronal processes. However, the other candidates cannot be excluded either. Earlier BXD studies identified significant QTLs for escape latency and number of annulus crossings in a spatial Morris water navigation task on Chr 1

(mapping to *Atp1a2* and most likely not related to learning *per se*, but to swimming speed; see Williams & Mulligan, 2012) and Chr 5 (Milhaud *et al.*, 2002). That different QTLs were obtained for learning performance in these two different tasks (radial maze and water navigation) is perhaps not too surprising. Learning will be influenced by mnemonic- and stress-related processes in task-dependent ways. For example, being forced to swim is very stressful for mice, which prefer dry-land tasks (Gerlai & Clayton, 1999, Whishaw, 1995, Whishaw & Tomie, 1996), so anxiety-related processes will influence test performance more in tasks requiring swimming than in dry-land tasks like the radial maze. Hence, different genetic correlates are to be expected.

Several significant and suggestive QTLs were identified for hippocampal morphometric variables. For the size of the IIPMF, we identified a significant QTL on the X chromosome affecting mossy fiber size. Further analysis reveals a single gene candidate in that region. The QTL on Chr 11 misses significance, but is highly suggestive. In addition, there is further evidence from the data obtained with the SRH/SRL selected inbred lines supporting the implication of this region. Based on functional association, *Gpc4* (Chr X) and *Tenm2/Odz2* (Chr 11) are strong candidates to modulate IIPMF size. Both genes encode glycoproteins that interact with the cell surface and extracellular matrix proteins like signaling receptors and morphogens. Both genes are also associated with neuronal processes.

Our findings for the IIPMF can be compared with those of an earlier study that had 18 BXD strains in common with ours (Lassalle *et al.*, 1999). A strong correlation was obtained between Lassalle et al.'s and our data (r=0.78, P<<0.001). Using pooled data from males and females, Lassalle *et al.* reported suggestive QTLs on Chr 10 and the X chromosome (Lassalle *et al.*, 1999). To compare the X-chromosomal QTL with the one reported here, we used WebQTL, where these authors had archived their raw data, to re-analyze the Lassalle data with the same methods as employed here. Surprisingly, the re-analysis (Fig. S14) only showed two QTLs on Chr 4 and 10 that barely crossed the suggestive LRS threshold. The Chr 10 QTL is located in about the middle of the chromosome, whereas the QTL reported by Lassalle *et al.* was at the distal end. The probable reason for these discrepancies is that, while Lassalle *et al.* used methods and gene-map data that were state-of-the-art when they performed their study, the genetic maps of the time contained many errors that have since been corrected (Williams *et al.*, 2001, Williams & Mulligan, 2012). Many additional BXD strains that have become available since Lassalle *et al.*'s work was published were used in the present study, greatly increasing power to detect loci. Taken together, this explains why Lassalle *et al.* did not find the suggestive and significant QTLs reported here. As we did not find even mildly suggestive QTLs on Chr 4 or 10, the low signals obtained in the present re-analysis of the Lassalle data most probably are a chance finding.

For the stratum pyramidale a significant QTL was found on Chr 11 and the suggestive QTL on Chr 11 for IIPMF size occurs in the same general region and overlaps somewhat, but its interval is narrower. A possible common gene for the sizes of the IIPMF and the stratum pyramidale is conceivable, given their functional anatomical relationship: the IIPMF are the synapses of the dentate gyrus granular cell axons upon the dendrites of the pyramidal cells.

The highly suggestive QTL for the size of the hilus on Chr 13 (106–108 Mb) occurs in a gene sparse region, yielding just one gene candidate, *Ipo11*. If the interval is extended to 106–112 Mb, then there are two additional candidate genes *Rab3c* and *Pde4d*. Each of these three genes is associated with learning and memory.

With the exception of the IIPMF (see above) none of the QTLs reported here overlap appreciably with those reported for other hippocampal variables in GeneNetwork, including volume and weight of the hippocampus, numbers of granule cells in the dentate gyrus, or levels of adult neurogenesis.

IIPMF and learning

No QTLs found here were shared between the neuroanatomical and behavioral variables. This is to be expected, given the low and non-significant correlation between morphometric traits and learning. The absence of correlations itself, however, is more surprising, given the fact that the strong correlation between the IIPMF and learning performance in a radial maze has been replicated many times by us and our collaborators in different laboratories (Crusio & Schwegler, 1991, Crusio & Schwegler, 2005, Crusio *et al.*, 1993, Crusio *et al.*, 1987, Schwegler & Crusio, 1995, Schwegler *et al.*, 1990, Schwegler *et al.*, 1991). There was some indication of the predicted relationship in that IIPMF and learning loaded on the same factor in the factor analysis (particularly in the males), but this is nevertheless much weaker than was anticipated. One obvious explanation for this discrepancy would be that our hypothesis of a causal relationship between the size of the IIPMF and radial maze learning is incorrect. However, given the strength of the evidence from our earlier studies, this seems unlikely.

Comparing the present results with those that we obtained earlier is only possible for C57BL/6J and DBA/2J, as this was the first time that BXD animals were tested in a radial maze. The large difference between C57BL/6 and DBA/2 in the sizes of their IIPMF projections reported here is completely consistent with our previous findings. In addition, our IIPMF measurements in the BXDs correlated strongly with those reported by Lassalle et al. (1999). It would therefore appear that it is our behavioral data that do not conform to what would have been expected. Indeed, the C57BL/6 animals in the present study clearly learned less well than those in previous studies. When we examine the totality of the BXD strains studied here, we note that many strains learned the task reasonably well, but, in fact, no strain was a really good learner (cf. Fig. S4). Given the large differences that we found previously (Crusio, 2013) between C57BL/6 and DBA/2, this is unexpected.

One possible explanation for the lower than expected performance of the C57BL/6 and (at least some) BXD strains lies in the housing conditions. Our animal facility was built to house about 500 cages in one large breeding room. However, the cage-washing installation (and the available personnel) could not handle that many cages at a time. As a result, every day one or two racks of cages were changed. C57BL/6 mice are sensitive to such disruptions and, indeed, breeding results were only mediocre. This also proved to be the case for several BXD strains. As a consequence we had to increase the number of breeding pairs for a number of strains, leading to an overcrowding of the facility (occasionally up to 650 cages). It is conceivable that the stress occasioned in the animal facility influenced later learning performance in a negative way, therefore obscuring the predicted correlation.

Gene interaction analysis

Two sub-network motifs were identified in the IIPMF gene interaction network. One of these motifs involves the *Tenm2* which emerged as a potential candidate for regulating IIPMF size. The second cluster contains *Ndufs8* which along with *Blc2l1*, bridges the IIPMF and pyramidale gene-expression networks. The remaining genes present in the motifs and merged graph are mainly involved in cell adhesion, cell growth and migration, neuronal-signaling, mitochondria redox reactions, and apoptosis. It is reasonable that the networks for the IIPMF and the stratum pyramidale intersect, given the anatomical relationship between the IIPMF and pyramidal cells discussed above. While there is no direct physical evidence for these interactions (like protein-protein interaction data), the functional association of these genes is understandable when one considers that apoptosis balances cell growth and proliferation and helps maintain tissue homeostasis which is highly relevant to the hippocampal measurements described here. Moreover, cellular energy demands are continually shifting during processes related to cytoskeletal rearrangements and these energy requirements are directly linked to ATP production via electron transfer/redox reactions in mitochondria by complexes like Mitochondrial complex 1. Indeed, genetically disrupting neuronal metabolism impedes memory formation in mice (Pei *et al.*, 2015).

Trait correlation analysis

The phenotypes in the GeneNetwork database that covary with the QTL data include a wide variety of traits related to morphology, behavior, and physiology, as well as immune system function. Common themes among the covariates include several traits from a study involving a Huntington model hybrid: open-field activity, ratio of soluble-aggregate protein, pre-pulse inhibition (PPI) of the acoustic startle response, and brain and body weight ratio. The PPI-hippocampus connection has been observed in a previous study that also considered hippocampal morphometric measures (Peirce *et al.*, 2003). An inverse correlation between dentate gyrus granule cell proliferation volume (trait ID 10460) and PPI was observed. This is a reasonable association considering transient disruption of hippocampal activity reduces PPI (Bast & Feldon, 2003, Zhang *et al.*, 2002). Other covariates are concerned with exploratory behavior and locomotor activities as well as anxiety and stress and these are all relevant to hippocampal function as well.

For the physiological covariates, which include brain metal ion levels (zinc, copper, iron), respiration and olfactory bulb activity, and Drd2 binding, it is well established that metal ions play a role in neuronal processes and neurodegenerative diseases like Alzheimer's, Parkinson’s, and others by causing protein misfolding and oxidative stress. Drd2 signaling has also been associated with hippocampal related processes like working memory and memory formation.

The relationship between hippocampal morphometry, radial maze learning, variables related to immune system function, and the response to various bacterial and viral infections is less obvious. However, there is an established, but as yet poorly understood, link between the immune and nervous systems. The two are connected at least in part through cytokines which are signaling molecules that regulate both systems. Cytokine receptors are found in many neuronal cell populations including the hippocampus where they play a role in

neurogenesis and learning and memory and may also provide the basis for the covariation with the hippocampal morphometry traits presented here (Arisi, 2014).

Conclusion

In this study, we have identified multiple loci and gene variants linked to either structural differences in the hippocampus or learning in a spatial radial maze task. Although several significant QTLs were localized, none were common between behavior and morphometrical variation. Strong candidate genes that may modulate intra- and infrapyramidal mossy fiber areas are *Gpc4* and *Tenm2*, but further experiments are needed to confirm their direct implication.

Supplementary Material

Refer to Web version on PubMed Central for supplementary material.

Acknowledgments

This study was supported by the following grants: NIMH R01 MH072920 to WEC, NIAAA U01 AA016662 and U01 AA013499 to RW. Drs. Sabine Spijker and August B. Smit (Free University of Amsterdam) from the NeuroBSIK Mouse Phenomics Consortium (BSIK03053) generously provided several BXD strains (for the origin of these strains, see Loos *et al.*, 2014). We thank Raphael Pineau and Laetitia Meran for expert animal care and Alexis Cornuez for help with behavioral testing and histology.

REFERENCES

Achouche J, Laccourreye O, de Gaudemar I, George B, Merland JJ, Tran Ba Huy P. Les fibromes nasopharyngiens intra et extracraniens. Apport de l'imagerie et etude de l'echec local. A propos de 34 patients. Ann. Otolaryngol. Chir. Cervicofac. 1992; 109:223–230. [PubMed: 1292377]

Akarsu S, Torun D, Bolu A, Erdem M, Kozan S, Ak M, Akar H, Uzun O. Mitochondrial complex I and III gene mRNA levels in schizophrenia, and their relationship with clinical features. J. Mol. Psychiatry. 2014; 2:6. [PubMed: 25713723]

Alberts R, Schughart K. QTLminer: identifying genes regulating quantitative traits. BMC Bioinform. 2010; 11:516.

Allen NJ, Bennett ML, Foo LC, Wang GX, Chakraborty C, Smith SJ, Barres BA. Astrocyte glypicans 4 and 6 promote formation of excitatory synapses via GluA1 AMPA receptors. Nature. 2012; 486:410–414. [PubMed: 22722203]

Andersen, P.; Morris, R.; Amaral, D.; Bliss, T.; O'Keefe, J. The Hippocampus Book. New York, NY, USA: Oxford University Press; 2007. p. xx+832

Arisi GM. Nervous and immune systems signals and connections: cytokines in hippocampus physiology and pathology. Epilepsy Behav. 2014; 38:43–47. [PubMed: 24534466]

Barber RP, Vaughn JE, Wimer RE, Wimer CC. Genetically-associated variations in the distribution of dentate granule cell synapses upon the pyramidal cell dendrites in mouse hippocampus. J. Comp. Neurol. 1974; 156:417–434. [PubMed: 4137683]

Bast T, Feldon J. Hippocampal modulation of sensorimotor processes. Progr. Neurobiol. 2003; 70:319–345.

Bastias-Candia S, Braidy N, Zolezzi JM, Inestrosa NC. Teneurins and Alzheimer's disease: A suggestive role for a unique family of proteins. Med. Hypotheses. 2015; 84:402–407. [PubMed: 25665860]

Basu R, Taylor MR, Williams ME. The classic cadherins in synaptic specificity. Cell Adh. Migr. (in press).

Battle DJ, Lau CK, Wan L, Deng H, Lotti F, Dreyfuss G. The Gemin5 protein of the SMN complex identifies snRNAs. Mol. Cell. 2006; 23:273–279. [PubMed: 16857593]

Becchetti A, Aracri P, Meneghini S, Brusco S, Amadeo A. The role of nicotinic acetylcholine receptors in autosomal dominant nocturnal frontal lobe epilepsy. Front. Physiol. 2015; 6:22. [PubMed: 25717303]

Castilla C, Flores ML, Medina R, Perez-Valderrama B, Romero F, Tortolero M, Japon MA, Saez C. Prostate cancer cell response to paclitaxel is affected by abnormally expressed securin PTTG1. Mol. Cancer Ther. 2014; 13:2372–2383. [PubMed: 25122070]

Chen D, Zhang R, Shen W, Fu H, Liu S, Sun K, Sun X. RPS12-specific shRNA inhibits the proliferation, migration of BGC823 gastric cancer cells with S100A4 as a downstream effector. Int. J. Oncol. 2013; 42:1763–1769. [PubMed: 23546393]

Chong SY, Rosenberg SS, Fancy SP, Zhao C, Shen YA, Hahn AT, McGee AW, Xu X, Zheng B, Zhang LI, Rowitch DH, Franklin RJ, Lu QR, Chan JR. Neurite outgrowth inhibitor Nogo-A establishes spatial segregation and extent of oligodendrocyte myelination. Proc. Natl. Acad. Sci. USA. 2012; 109:1299–1304. [PubMed: 22160722]

Chozick BS. The behavioral effects of lesions of the hippocampus: a review. International Journal of Neuroscience. 1983; 22:63–80. [PubMed: 6365818]

Crusio WE. A note on the effect of within-strain sample sizes on QTL mapping in recombinant inbred strain studies. Genes Brain Behav. 2004; 3:249–251. [PubMed: 15248870]

Crusio, WE. Radial maze. In: Crusio, WE.; Sluyter, F.; Gerlai, RT.; Pietropaolo, S., editors. Behavioral Genetics of the Mouse: Genetics of Behavioral Phenotypes. Cambridge, United Kingdom: Cambridge University Press; 2013. p. 299-303.

Crusio WE, Genthner-Grimm G, Schwegler H. A quantitative-genetic analysis of hippocampal variation in the mouse. J. Neurogenet. 1986; 3:203–214. [PubMed: 3746523]

Crusio WE, Schwegler H. Early postnatal hyperthyroidism improves both working and reference memory in a spatial radial-maze task in adult mice. Physiol. Behav. 1991; 50:259–261. [PubMed: 1946727]

Crusio WE, Schwegler H. Learning spatial orientation tasks in the radial-maze and structural variation in the hippocampus in inbred mice. Behav. Brain Func. 2005; 1:3.

Crusio WE, Schwegler H, Brust I. Covariations between hippocampal mossy fibres and working and reference memory in spatial and non-spatial radial maze tasks in mice. Eur. J. Neurosci. 1993; 5:1413–1420. [PubMed: 8275238]

Crusio WE, Schwegler H, Brust I, van Abeelen JHF. Genetic selection for novelty-induced rearing behavior in mice produces changes in hippocampal mossy fiber distributions. J. Neurogenet. 1989; 5:87–93. [PubMed: 2703943]

Crusio WE, Schwegler H, Lipp H-P. Radial-maze performance and structural variation of the hippocampus in mice: a correlation with mossy fibre distribution. Brain Res. 1987; 425:182–185. [PubMed: 3427419]

Cusco I, Medrano A, Gener B, Vilardell M, Gallastegui F, Villa O, Gonzalez E, Rodriguez-Santiago B, Vilella E, Del Campo M, Perez-Jurado LA. Autism-specific copy number variants further implicate the phosphatidylinositol signaling pathway and the glutamatergic synapse in the etiology of the disorder. Hum. Mol. Genet. 2009; 18:1795–1804. [PubMed: 19246517]

Dai Y, Grant S. BCL2L11/Bim as a dual-agent regulating autophagy and apoptosis in drug resistance. Autophagy. 2015; 11:416–418. [PubMed: 25700997]

Danscher G, Zimmer J. An improved Timm sulphide silver method for light and electron microscopic localization of heavy metals in biological tissues. Histochemistry. 1978; 55:27–40. [PubMed: 76622]

Enkhmandakh B, Makeyev AV, Bayarsaihan D. The role of the proline-rich domain of Ssdp1 in the modular architecture of the vertebrate head organizer. Proc. Natl. Acad. Sci. USA. 2006; 103:11631–11636. [PubMed: 16864769]

Fico A, Maina F, Dono R. Fine-tuning of cell signaling by glypicans. Cell. Mol. Life Sci. 2011; 68:923–929. [PubMed: 18087675]

Filmus J, Capurro M. The role of glypicans in Hedgehog signaling. Matrix Biol. 2014; 35:248–252. [PubMed: 24412155]

Filmus J, Selleck SB. Glypicans: proteoglycans with a surprise. J. Clin. Invest. 2001; 108:497–501. [PubMed: 11518720]

Forwood JK, Lam MH, Jans DA. Nuclear import of Creb and AP-1 transcription factors requires importin-beta 1 and Ran but is independent of importin-alpha. Biochemistry. 2001; 40:5208–5217. [PubMed: 11318643]

Garzon J, Herrero-Labrador R, Rodriguez-Munoz M, Shah R, Vicente-Sanchez A, Wagner CR, Sanchez-Blazquez P. HINT1 protein: a new therapeutic target to enhance opioid antinociception and block mechanical allodynia. Neuropharmacology. 2015; 89:412–423. [PubMed: 25445489]

Gerlai R, Clayton NS. Analysing hippocampal function in transgenic mice: an ethological perspective. Trends Neurosci. 1999; 22:47–51. [PubMed: 10092042]

Grupe A, Li Y, Rowland C, Nowotny P, Hinrichs AL, Smemo S, Kauwe JS, Maxwell TJ, Cherny S, Doil L, Tacey K, van Luchene R, Myers A, Wavrant-De Vrieze F, Kaleem M, Hollingworth P, Jehu L, Foy C, Archer N, Hamilton G, Holmans P, Morris CM, Catanese J, Sninsky J, White TJ, Powell J, Hardy J, O'Donovan M, Lovestone S, Jones L, Morris JC, Thal L, Owen M, Williams J, Goate A. A scan of chromosome 10 identifies a novel locus showing strong association with late-onset Alzheimer disease. Am. J. Hum. Genet. 2006; 78:78–88. [PubMed: 16385451]

GTEx Consortium. Human genomics. The Genotype-Tissue Expression (GTEx) pilot analysis: multitissue gene regulation in humans. Science. 2015; 348:648–660. [PubMed: 25954001]

Gubitz AK, Mourelatos Z, Abel L, Rappsilber J, Mann M, Dreyfuss G. Gemin5, a novel WD repeat protein component of the SMN complex that binds Sm proteins. J. Biol. Chem. 2002; 277:5631–5636. [PubMed: 11714716]

Ha JY, Kim JS, Kang YH, Bok E, Kim YS, Son JH. Tnfaip8 l1/Oxi-beta binds to FBXW5, increasing autophagy through activation of TSC2 in a Parkinson's disease model. J. Neurochem. 2014; 129:527–538. [PubMed: 24444419]

Hager R, Lu L, Rosen GD, Williams RW. Genetic architecture supports mosaic brain evolution and independent brain-body size regulation. Nat. Commun. 2012; 3:1079. [PubMed: 23011133]

Harrington MG, Fonteh AN, Biringer RG, AF RH, Cowan RP. Prostaglandin D synthase isoforms from cerebrospinal fluid vary with brain pathology. Dis. Markers. 2006; 22:73–81. [PubMed: 16410653]

Hegmann JP, Possidente B. Estimating genetic correlations from inbred strains. Behav. Genet. 1981; 11:103–114. [PubMed: 7271677]

Herault Y, Michel D, Chatelain G, Brun G. cDNA and predicted amino acid sequences of the human ribosomal protein genes rpS12 and rpL17. Nucleic Acids Res. 1991; 19:4001. [PubMed: 1861993]

Hirose S. Mutant GABA(A) receptor subunits in genetic (idiopathic) epilepsy. Progr. Brain Res. 2014; 213:55–85.

Jackson KJ, Wang JB, Barbier E, Chen X, Damaj MI. Acute behavioral effects of nicotine in male and female HINT1 knockout mice. Genes Brain Behav. 2012; 11:993–1000. [PubMed: 22827509]

Ji CN, Chen JZ, Xie Y, Wang S, Qian J, Zhao E, Jin W, Wu XZ, Xu WX, Ying K, Mao YM. A novel cDNA encodes a putative hRALY-like protein, hRALYL. Mol. Biol. Rep. 2003; 30:61–67. [PubMed: 12688537]

Kash TL, Jenkins A, Kelley JC, Trudell JR, Harrison NL. Coupling of agonist binding to channel gating in the GABA(A) receptor. Nature. 2003; 421:272–275. [PubMed: 12529644]

Kenzelmann D, Chiquet-Ehrismann R, Leachman NT, Tucker RP. Teneurin-1 is expressed in interconnected regions of the developing brain and is processed in vivo. BMC Dev. Biol. 2008; 8:30. [PubMed: 18366734]

Lambert N, Robertson A, Jangi M, McGeary S, Sharp PA, Burge CB. RNA Bind-n-Seq: quantitative assessment of the sequence and structural binding specificity of RNA binding proteins. Mol. Cell. 2014; 54:887–900. [PubMed: 24837674]

Lassalle J-M, Halley H, Milhaud J-M, Roullet P. Genetic architecture of the hippocampal mossy fiber subfields in the BXD RI mouse strain series: A preliminary QTL analysis. Behav. Genet. 1999; 29:273–282.

Li W, Tao R, Zhang X, Ju G, Shi J, Liu S, Wang Z, Jin S, Guo Y, Wei J. A family-based study of genetic association of the PTGDS gene with schizophrenia in a Chinese population. Psychiatr. Genet. 2008; 18:99. [PubMed: 18349703]

Li YF, Cheng YF, Huang Y, Conti M, Wilson SP, O'Donnell JM, Zhang HT. Phosphodiesterase-4D knock-out and RNA interference-mediated knock-down enhance memory and increase hippocampal neurogenesis via increased cAMP signaling. J. Neurosci. 2011; 31:172–183. [PubMed: 21209202]

Lindskog S. Structure and mechanism of carbonic anhydrase. Pharmacol. Ther. 1997; 74:1–20. [PubMed: 9336012]

Loos M, Mueller T, Gouwenberg Y, Wijnands R, van der Loo RJ, Birchmeier C, Smit AB, Spijker S. Neuregulin-3 in the mouse medial prefrontal cortex regulates impulsive action. Biol. Psychiatry. 2014; 76:648–655. [PubMed: 24703509]

Lu H, Yu Z, Liu S, Cui L, Chen X, Yao R. CUGBP1 promotes cell proliferation and suppresses apoptosis via down-regulating C/EBPalpha in human non-small cell lung cancers. Med. Oncol. 2015; 32:82. [PubMed: 25701464]

Lu L, Airey DC, Williams RW. Complex trait analysis of the hippocampus: mapping and biometric analysis of two novel gene loci with specific effects on hippocampal structure in mice. J. Neurosci. 2001; 21:3503–3514. [PubMed: 11331379]

Maguire EA, Spiers HJ, Good CD, Hartley T, Frackowiak RS, Burgess N. Navigation expertise and the human hippocampus: a structural brain imaging analysis. Hippocampus. 2003; 13:250–259. [PubMed: 12699332]

Mancuso M, Calsolaro V, Orsucci D, Carlesi C, Choub A, Piazza S, Siciliano G. Mitochondria, cognitive impairment, and Alzheimer's disease. Int. J. Alzheimers Dis. 2009; 2009:951548. [PubMed: 20798880]

Martins-de-Souza D, Guest PC, Harris LW, Vanattou-Saifoudine N, Webster MJ, Rahmoune H, Bahn S. Identification of proteomic signatures associated with depression and psychotic depression in post-mortem brains from major depression patients. Transl. Psychiatry. 2012; 2:e87. [PubMed: 22832852]

Milhaud JM, Halley H, Lassalle J-M. Two QTLs located on chromosomes 1 and 5 modulate different aspects of the performance of mice of the B×D Ty RI strain series in the Morris navigation task. Behav. Genet. 2002; 32:69–78. [PubMed: 11958544]

Nakamichi N, Taguchi T, Hosotani H, Wakayama T, Shimizu T, Sugiura T, Iseki S, Kato Y. Functional expression of carnitine/organic cation transporter OCTN1 in mouse brain neurons: possible involvement in neuronal differentiation. Neurochem. Int. 2012; 61:1121–1132. [PubMed: 22944603]

Nishioka N, Nagano S, Nakayama R, Kiyonari H, Ijiri T, Taniguchi K, Shawlot W, Hayashizaki Y, Westphal H, Behringer RR, Matsuda Y, Sakoda S, Kondoh H, Sasaki H. Ssdp1 regulates head morphogenesis of mouse embryos by activating the Lim1-Ldb1 complex. Development. 2005; 132:2535–2546. [PubMed: 15857913]

Nunes SM, Ferralli J, Choi K, Brown-Luedi M, Minet AD, Chiquet-Ehrismann R. The intracellular domain of teneurin-1 interacts with MBD1 and CAP/ponsin resulting in subcellular codistribution and translocation to the nuclear matrix. Exp. Cell Res. 2005; 305:122–132. [PubMed: 15777793]

O'Keefe, J.; Nadel, L. The Hippocampus as a Cognitive Map. Oxford: Clarendon Press; 1978.

Olton DS, Samuelson RJ. Remembrance of places passed: spatial memory in rats. J. Exp. Psychol. Anim. Behav. Process. 1976; 2:97–117.

Oohashi T, Zhou XH, Feng K, Richter B, Morgelin M, Perez MT, Su WD, Chiquet-Ehrismann R, Rauch U, Fassler R. Mouse ten-m/Odz is a new family of dimeric type II transmembrane proteins expressed in many tissues. J. Cell Biol. 1999; 145:563–577. [PubMed: 10225957]

Pei L, Mu Y, Leblanc M, Alaynick W, Barish GD, Pankratz M, Tseng TW, Kaufman S, Liddle C, Yu RT, Downes M, Pfaff SL, Auwerx J, Gage FH, Evans RM. Dependence of hippocampal function on ERRgamma-regulated mitochondrial metabolism. Cell Metab. 2015; 21:628–636. [PubMed: 25863252]

Peirce JL, Chesler EJ, Williams RW, Lu L. Genetic architecture of the mouse hippocampus: identification of gene loci with selective regional effects. Genes Brain Behav. 2003; 2:238–252. [PubMed: 12953790]

Peirce JL, Lu L, Gu J, Silver LM, Williams RW. A new set of BXD recombinant inbred lines from advanced intercross populations in mice. BMC Genet. 2004; 5:7. [PubMed: 15117419]

Procaccio V, Wallace DC. Late-onset Leigh syndrome in a patient with mitochondrial complex I NDUFS8 mutations. Neurology. 2004; 62:1899–1901. [PubMed: 15159508]

Putcha GV, Moulder KL, Golden JP, Bouillet P, Adams JA, Strasser A, Johnson EM. Induction of BIM, a proapoptotic BH3-only BCL-2 family member, is critical for neuronal apoptosis. Neuron. 2001; 29:615–628. [PubMed: 11301022]

Raiker SJ, Lee H, Baldwin KT, Duan Y, Shrager P, Giger RJ. Oligodendrocyte-myelin glycoprotein and Nogo negatively regulate activity-dependent synaptic plasticity. J. Neurosci. 2010; 30:12432–12445. [PubMed: 20844138]

Rodriguez-Munoz M, Sanchez-Blazquez P, Herrero-Labrador R, Martinez-Murillo R, Merlos M, Vela JM, Garzon J. The sigma1 receptor engages the redox-regulated HINT1 protein to bring opioid analgesia under NMDA receptor negative control. Antioxid. Redox Signal. 2015; 22:799–818. [PubMed: 25557043]

Rubin BP, Tucker RP, Martin D, Chiquet-Ehrismann R. Teneurins: a novel family of neuronal cell surface proteins in vertebrates, homologous to the Drosophila pair-rule gene product Ten-m. Dev. Biol. 1999; 216:195–209. [PubMed: 10588872]

Rutten K, Misner DL, Works M, Blokland A, Novak TJ, Santarelli L, Wallace TL. Enhanced long-term potentiation and impaired learning in phosphodiesterase 4D-knockout (PDE4D) mice. Eur. J. Neurosci. 2008; 28:625–632. [PubMed: 18702734]

Ruusuvuori E, Huebner AK, Kirilkin I, Yukin AY, Blaesse P, Helmy M, Kang HJ, El Muayed M, Hennings JC, Voipio J, Sestan N, Hubner CA, Kaila K. Neuronal carbonic anhydrase VII provides GABAergic excitatory drive to exacerbate febrile seizures. EMBO J. 2013; 32:2275–2286. [PubMed: 23881097]

Saghazadeh A, Mastrangelo M, Rezaei N. Genetic background of febrile seizures. Rev. Neurosci. 2014; 25:129–161. [PubMed: 24399675]

Sakane H, Yamamoto H, Matsumoto S, Sato A, Kikuchi A. Localization of glypican-4 in different membrane microdomains is involved in the regulation of Wnt signaling. J. Cell. Sci. 2012; 125:449–460. [PubMed: 22302992]

Schluter OM, Basu J, Sudhof TC, Rosenmund C. Rab3 superprimes synaptic vesicles for release: implications for short-term synaptic plasticity. J. Neurosci. 2006; 26:1239–1246. [PubMed: 16436611]

Schluter OM, Schmitz F, Jahn R, Rosenmund C, Sudhof TC. A complete genetic analysis of neuronal Rab3 function. J. Neurosci. 2004; 24:6629–6637. [PubMed: 15269275]

Schwegler H, Crusio WE. Correlations between radial-maze learning and structural variations of septum and hippocampus in rodents. Behav. Brain Res. 1995; 67:29–41. [PubMed: 7748498]

Schwegler H, Crusio WE, Brust I. Hippocampal mossy fibers and radial-maze learning in the mouse: a correlation with spatial working memory but not with non-spatial reference memory. Neuroscience. 1990; 34:293–298. [PubMed: 2333144]

Schwegler H, Crusio WE, Lipp H-P, Brust I, Mueller GG. Early postnatal hyperthyroidism alters hippocampal circuitry and improves radial-maze learning in adult mice. J. Neurosci. 1991; 11:2102–2106. [PubMed: 2066776]

Serralbo O, Marcelle C. Migrating cells mediate long-range WNT signaling. Development. 2014; 141:2057–2063. [PubMed: 24803654]

Sherry DF, Jacobs LF, Gaulin SJC. Spatial memory and adaptive specialization of the hippocampus. Trends Neurosci. 1992; 15:298–303. [PubMed: 1384199]

Shettleworth SJ. Varieties of learning and memory in animals. J. Exp. Psychol. Anim. Behav. Process. 1993; 19:5–14. [PubMed: 8418217]

Siegel, S. Nonparametric Statistics for the Behavioral Sciences. New York: McGraw-Hill; 1956.

Sofola OA, Jin P, Qin Y, Duan R, Liu H, de Haro M, Nelson DL, Botas J. RNA-binding proteins hnRNP A2/B1 and CUGBP1 suppress fragile X CGG premutation repeat-induced neurodegeneration in a *Drosophila* model of FXTAS. Neuron. 2007; 55:565–571. [PubMed: 17698010]

Sohn SJ, Rajpal A, Winoto A. Apoptosis during lymphoid development. Curr. Opin. Immunol. 2003; 15:209–216. [PubMed: 12633672]

Song L, Cortopassi G. Mitochondrial complex I defects increase ubiquitin in substantia nigra. Brain Res. 2015; 1594:82–91. [PubMed: 25446449]

Steeb H, Ramsey JM, Guest PC, Stocki P, Cooper JD, Rahmoune H, Ingudomnukul E, Auyeung B, Ruta L, Baron-Cohen S, Bahn S. Serum proteomic analysis identifies sex-specific differences in lipid metabolism and inflammation profiles in adults diagnosed with Asperger syndrome. Mol. Autism. 2014; 5:4. [PubMed: 24467795]

Tong Y, Ben-Shlomo A, Zhou C, Wawrowsky K, Melmed S. Pituitary tumor transforming gene 1 regulates Aurora kinase A activity. Oncogene. 2008; 27:6385–6395. [PubMed: 18663361]

Tsetsenis T, Younts TJ, Chiu CQ, Kaeser PS, Castillo PE, Sudhof TC. Rab3B protein is required for long-term depression of hippocampal inhibitory synapses and for normal reversal learning. Proc. Natl. Acad. Sci. USA. 2011; 108:14300–14305. [PubMed: 21844341]

van Abeelen JHF. Genetics of rearing behavior in mice. Behav. Genet. 1970; 1:71–76. [PubMed: 5527374]

Vawter MP, Crook JM, Hyde TM, Kleinman JE, Weinberger DR, Becker KG, Freed WJ. Microarray analysis of gene expression in the prefrontal cortex in schizophrenia: a preliminary study. Schizophr. Res. 2002; 58:11–20. [PubMed: 12363385]

Wagstaff KM, Jans DA. Importins and beyond: non-conventional nuclear transport mechanisms. Traffic. 2009; 10:1188–1198. [PubMed: 19548983]

Waizenegger I, Gimenez-Abian JF, Wernic D, Peters JM. Regulation of human separase by securin binding and autocleavage. Curr. Biol. 2002; 12:1368–1378. [PubMed: 12194817]

Wang L, Jiao Y, Cao Y, Liu G, Wang Y, Gu W. Limitation of number of strains and persistence of false positive loci in QTL mapping using recombinant inbred strains. PLoS ONE. 2014; 9:e102307. [PubMed: 25032693]

Wang XN, Agarwala R, Capra JA, Chen Z, Church DM, Ciobanu DC, Li ZW, Lu L, Mozhui K, Mulligan MK, Nelson SF, Pollard KS, Taylor WL, Thomason DB, Williams RW. High-throughput sequencing of the DBA/2J mouse genome. BMC Bioinform. 2010; 11:O7.

Whishaw IQ. A comparison of rats and mice in a swimming pool place task and matching to place task: some surprising differences. Physiol. Behav. 1995; 58:687–693. [PubMed: 8559777]

Whishaw IQ, Tomie JA. Of mice and mazes: similarities between mice and rats on dry land but not water mazes. Physiol. Behav. 1996; 60:1191–1197. [PubMed: 8916170]

Williams RW, Gu J, Qi S, Lu L. The genetic structure of recombinant inbred mice: high-resolution consensus maps for complex trait analysis. Genome Biol. 2001; 2:1–18.

Williams RW, Mulligan MK. Genetic and molecular network analysis of behavior. International Review of Neurobiology. 2012; 104:135–157. [PubMed: 23195314]

Xu S. Theoretical basis of the Beavis effect. Genetics. 2003; 165:2259–2268. [PubMed: 14704201]

Yan Z, Zou H, Tian F, Grandis JR, Mixson AJ, Lu PY, Li LY. Human rhomboid family-1 gene silencing causes apoptosis or autophagy to epithelial cancer cells and inhibits xenograft tumor growth. Mol. Cancer Ther. 2008; 7:1355–1364. [PubMed: 18524845]

Yin KJ, Hsu CY, Hu XY, Chen H, Chen SW, Xu J, Lee JM. Protein phosphatase 2A regulates bim expression via the Akt/FKHRL1 signaling pathway in amyloid-beta peptide-induced cerebrovascular endothelial cell death. J. Neurosci. 2006; 26:2290–2299. [PubMed: 16495456]

Yoon CH, Kim MJ, Lee H, Kim RK, Lim EJ, Yoo KC, Lee GH, Cui YH, Oh YS, Gye MC, Lee YY, Park IC, An S, Hwang SG, Park MJ, Suh Y, Lee SJ. PTTG1 oncogene promotes tumor malignancy via epithelial to mesenchymal transition and expansion of cancer stem cell population. J. Biol. Chem. 2012; 287:19516–19527. [PubMed: 22511756]

Young TR, Leamey CA. Teneurins: important regulators of neural circuitry. Int. J. Biochem. Cell Biol. 2009; 41:990–993. [PubMed: 18723111]

Zhang WN, Bast T, Feldon J. Prepulse inhibition in rats with temporary inhibition/inactivation of ventral or dorsal hippocampus. Pharmacol. Biochem. Behav. 2002; 73:929–940. [PubMed: 12213540]

Zhou XH, Brandau O, Feng K, Oohashi T, Ninomiya Y, Rauch U, Fassler R. The murine Ten-m/Odz genes show distinct but overlapping expression patterns during development and in adult brain. Gene Expr. Patterns. 2003; 3:397–405. [PubMed: 12915301]

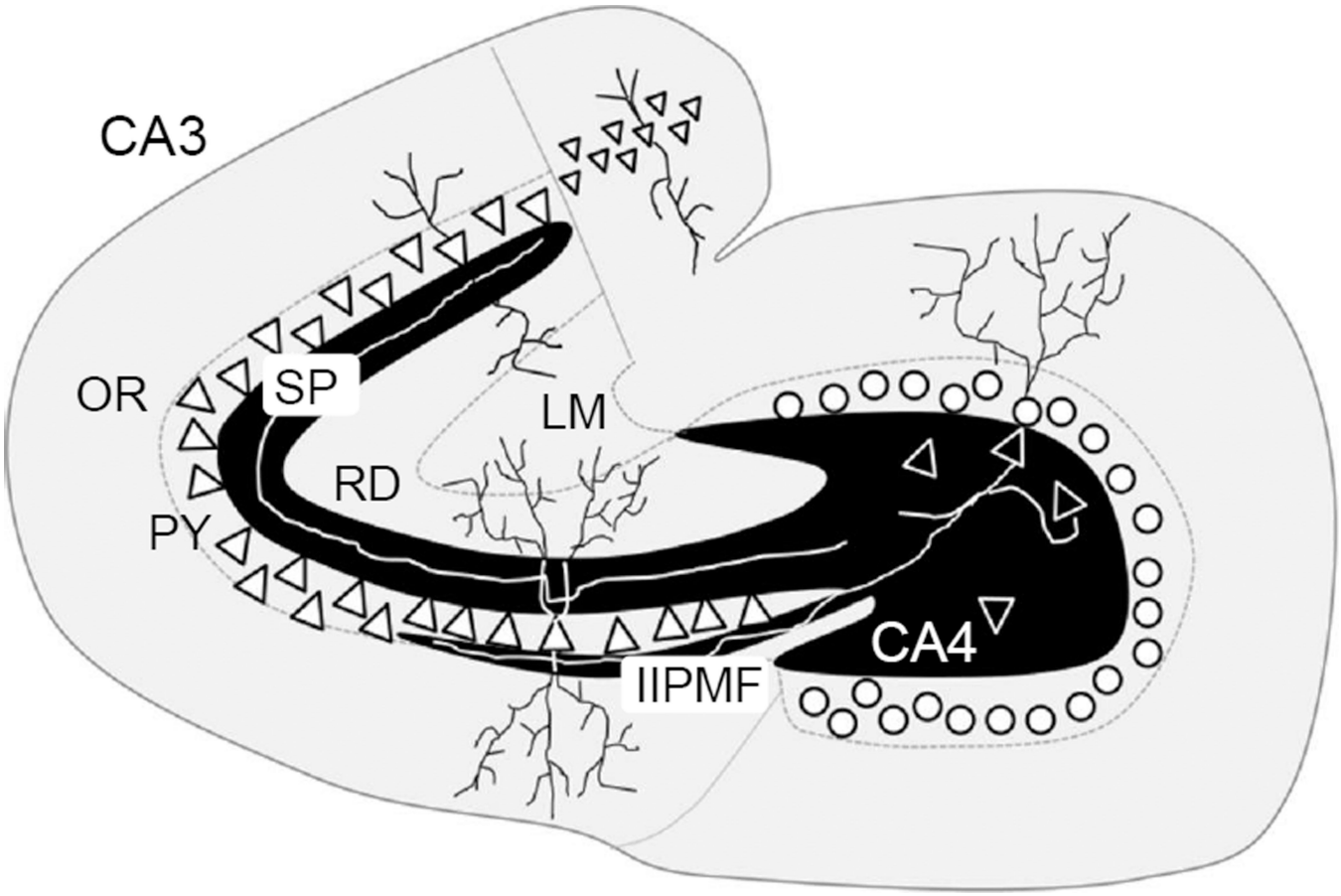

Figure 1. Schematic diagram of the mouse hippocampus

Shown are the 7 hippocampal fields measured in this study; suprapyramidal mossy fibers (SP), stratum oriens (OR), stratum pyramidale (PY), stratum radiatum (RD), stratum lacunosum-moleculare (LM), Hilus (CA4), intra- and infrapyramidal mossy fibers (IIPMF).

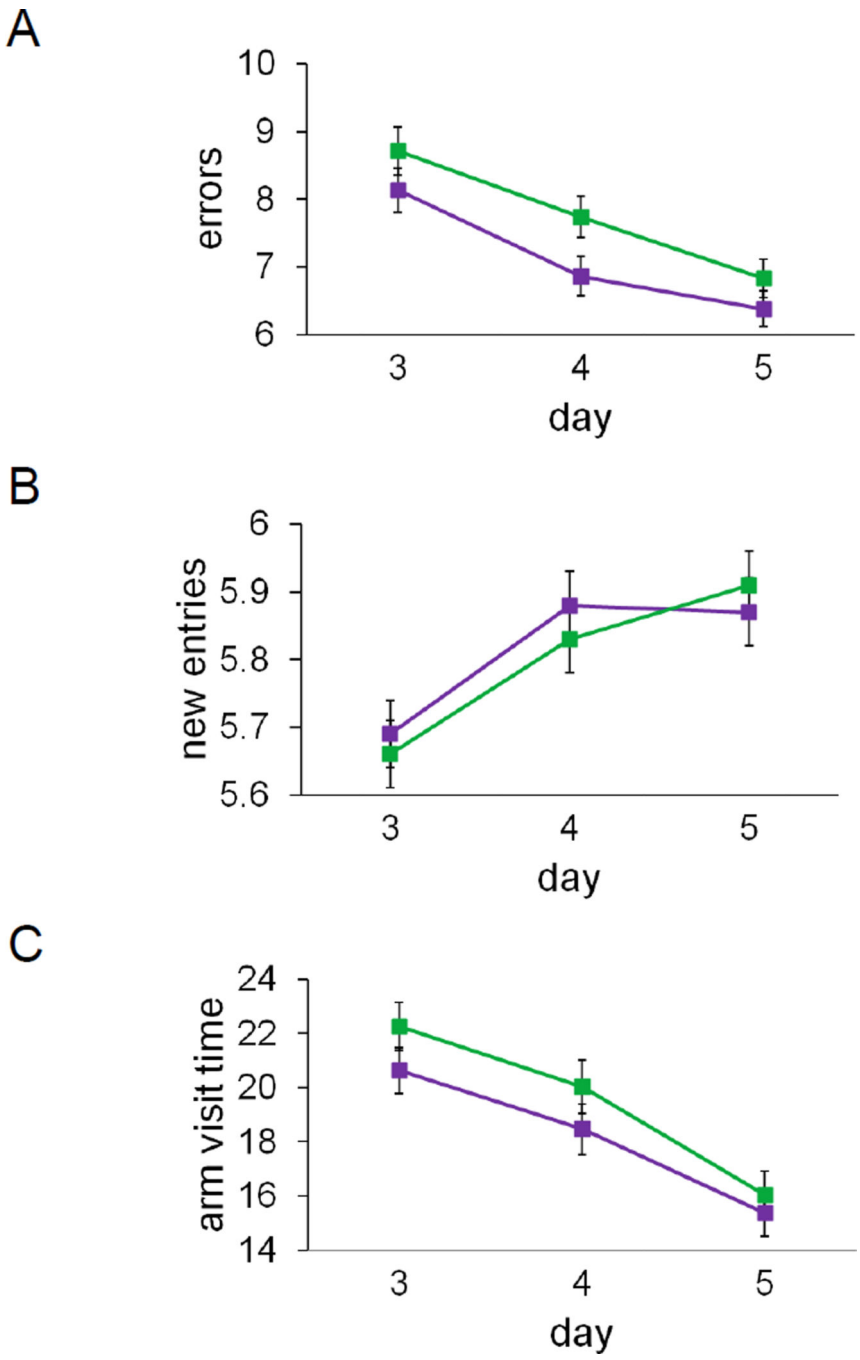

Figure 2. Radial maze learning in male and female mice

A: least square means of total number of errors made, B: new entries, and C: arm visit time (seconds) for days 3–5 (x-axis) of radial maze testing. Males: purple, females: yellow. Error bars represent +/− SEM.

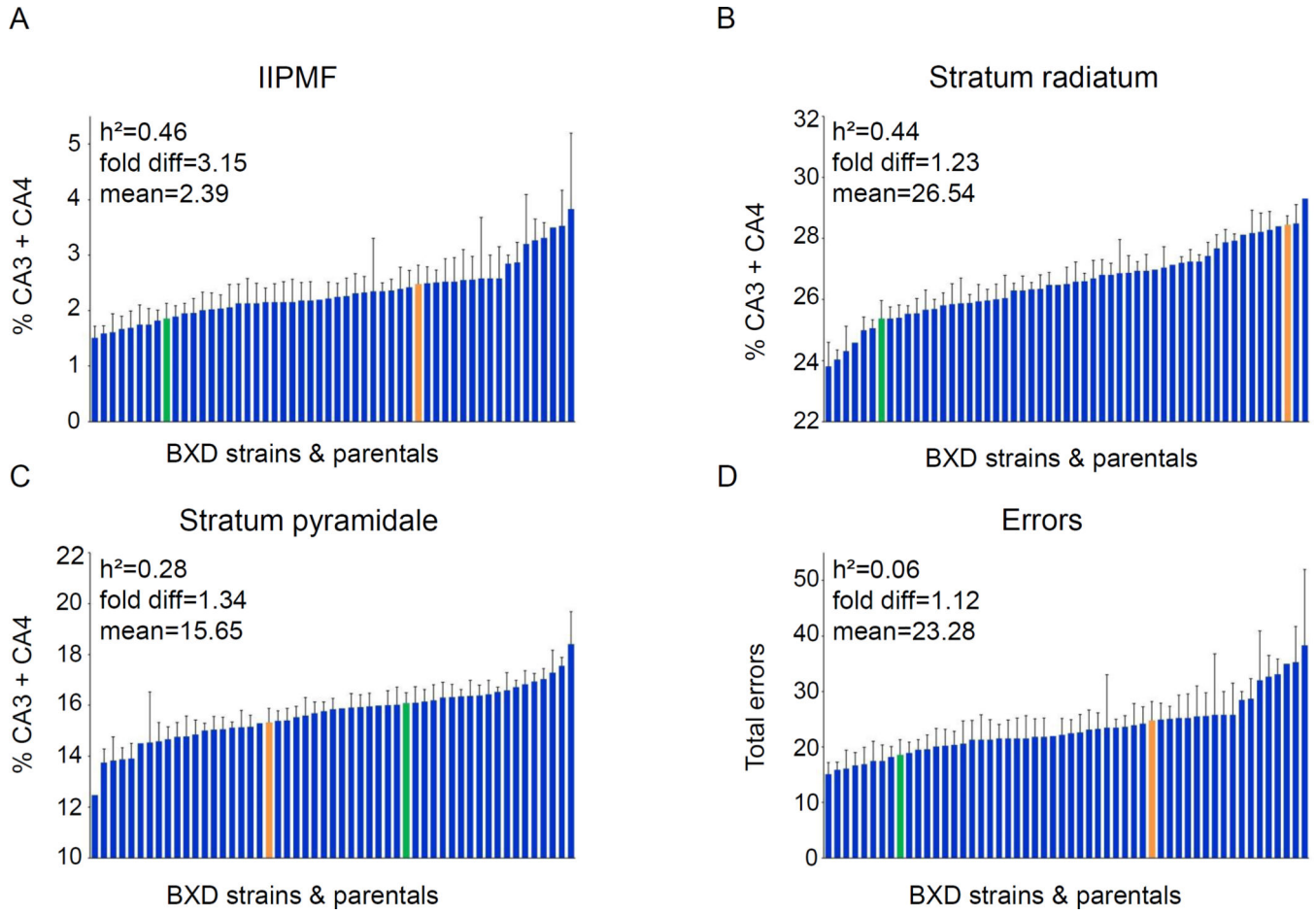

Figure 3. BXD strain differences in hippocampal morphometry and radial maze learning

Variation in the sizes of hippocampal subfields in the BXD and the parental strains (C57BL/6J: green bars and DBA/2J: orange bars) for the IIPMF (A), Stratum radiatum (B), and Stratum pyramidale (C) along with the spatial learning trait, errors (D). Bar graphs represent the means (+/− SEM). Heritability (h^2), fold difference, and overall mean are shown for each trait. The y-axis represents percentage of total CA3+CA4 and the x-axis lists the BXD strains (rank ordered from low to high).

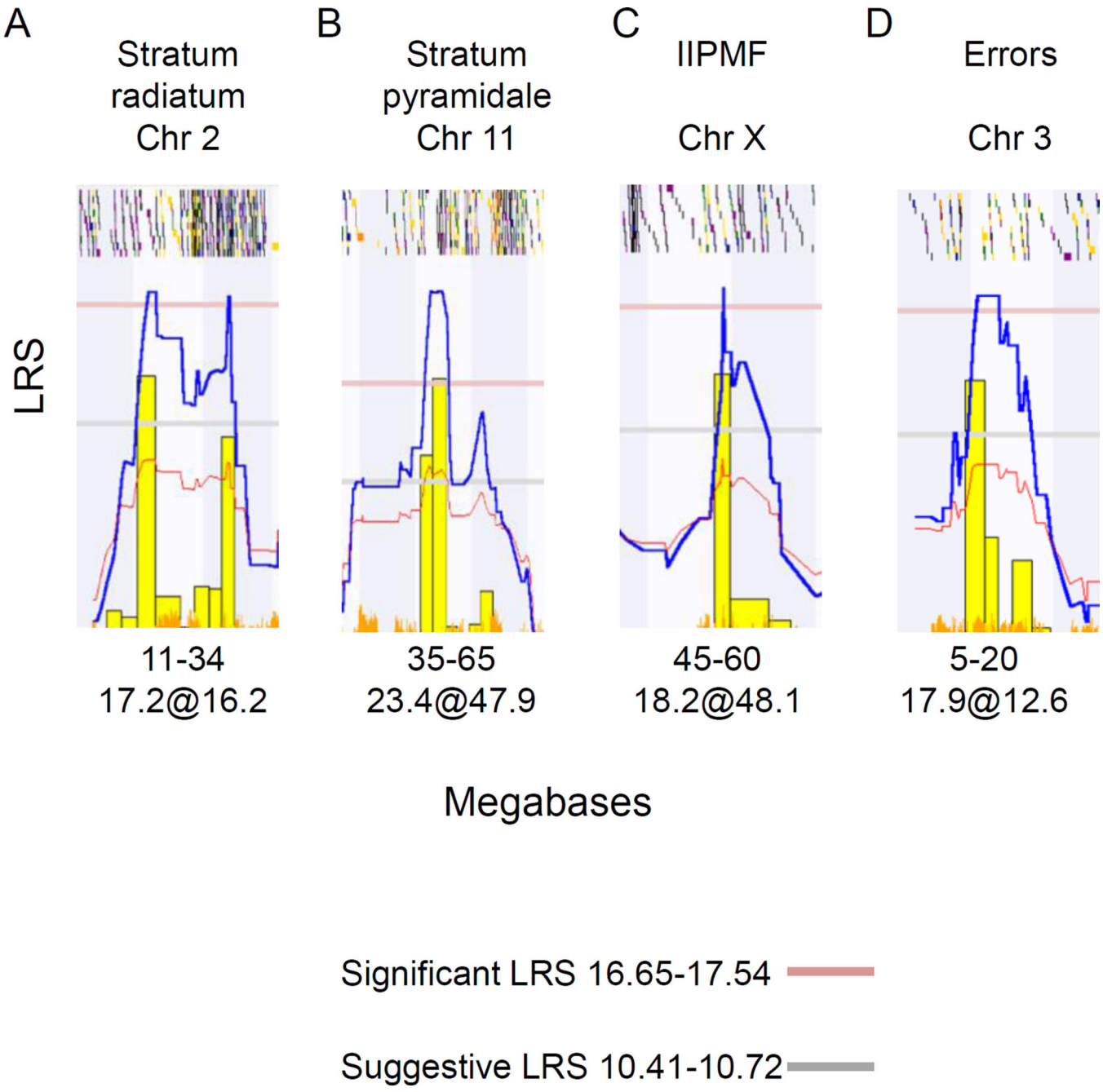

Figure 4. QTL graphs of hippocampal morphometry and radial maze learning

Graphs indicating the chromosomal loci that modulate A: Stratum radiatum (males), b: Stratum pyramidale (females), and C: IIPMF (males) sizes along with D: Errors in the radial maze (females). The x-axis represents megabase position. The y-axis represents the likelihood ratio statistic (LRS) of linkage. Blue lines represent LRS across the genome. The pink and gray horizontal lines are approximate threshold values which are used to assess whether a peak is significant ($P<0.05$) or suggestive ($P<0.63$), respectively. Colored rectangles depict individual genes, red and green lines represent the additive genetic contribution; red lines indicate negative values (C57BL/6J alleles increasing trait values) and

green lines indicate positive values (DBA/2J alleles increasing trait values). Gray lines are shown when the parental strain is unknown. The orange hash marks on the x-axis signify the SNP density (sequence difference between the two parental strains). The yellow bars represent the relative frequency of peak LRS at a given location from 2000 bootstrap resamples. Below the x-axis legend the peak LRS and its position is indicated.

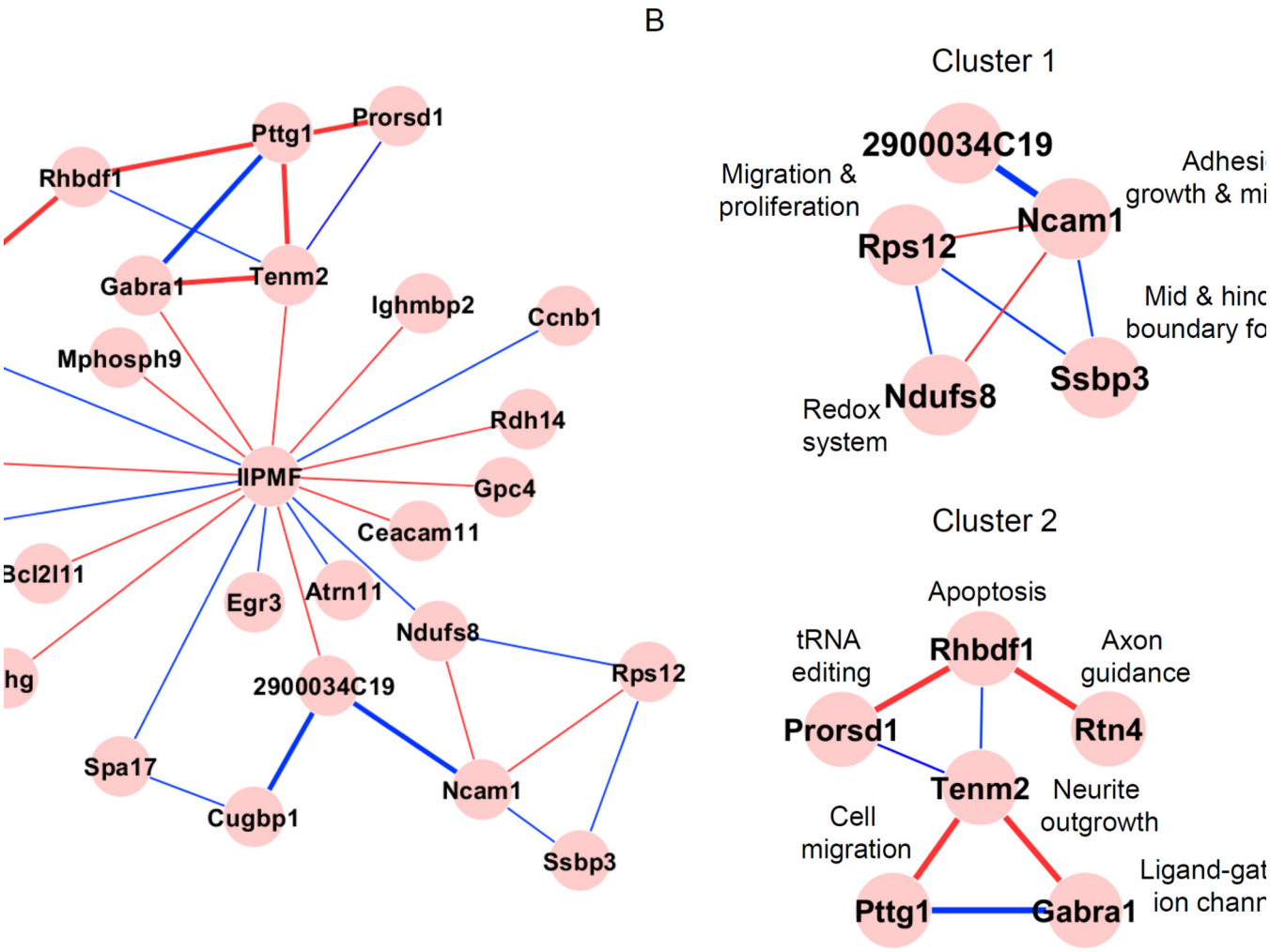

Figure 5. Hippocampal mRNAs associated with IIPMF size

A: Network graph of the IIPMF together with the respective top mRNA covariates expressed in the hippocampus. Edges are colored either red or blue to highlight negative and positive correlations, respectively. Line thickness represents correlation strength. B: The IIPMF graph has two subnetwork clusters (cluster 1, top; cluster 2, bottom) that are highly interconnected and contain some of the strongest correlates.

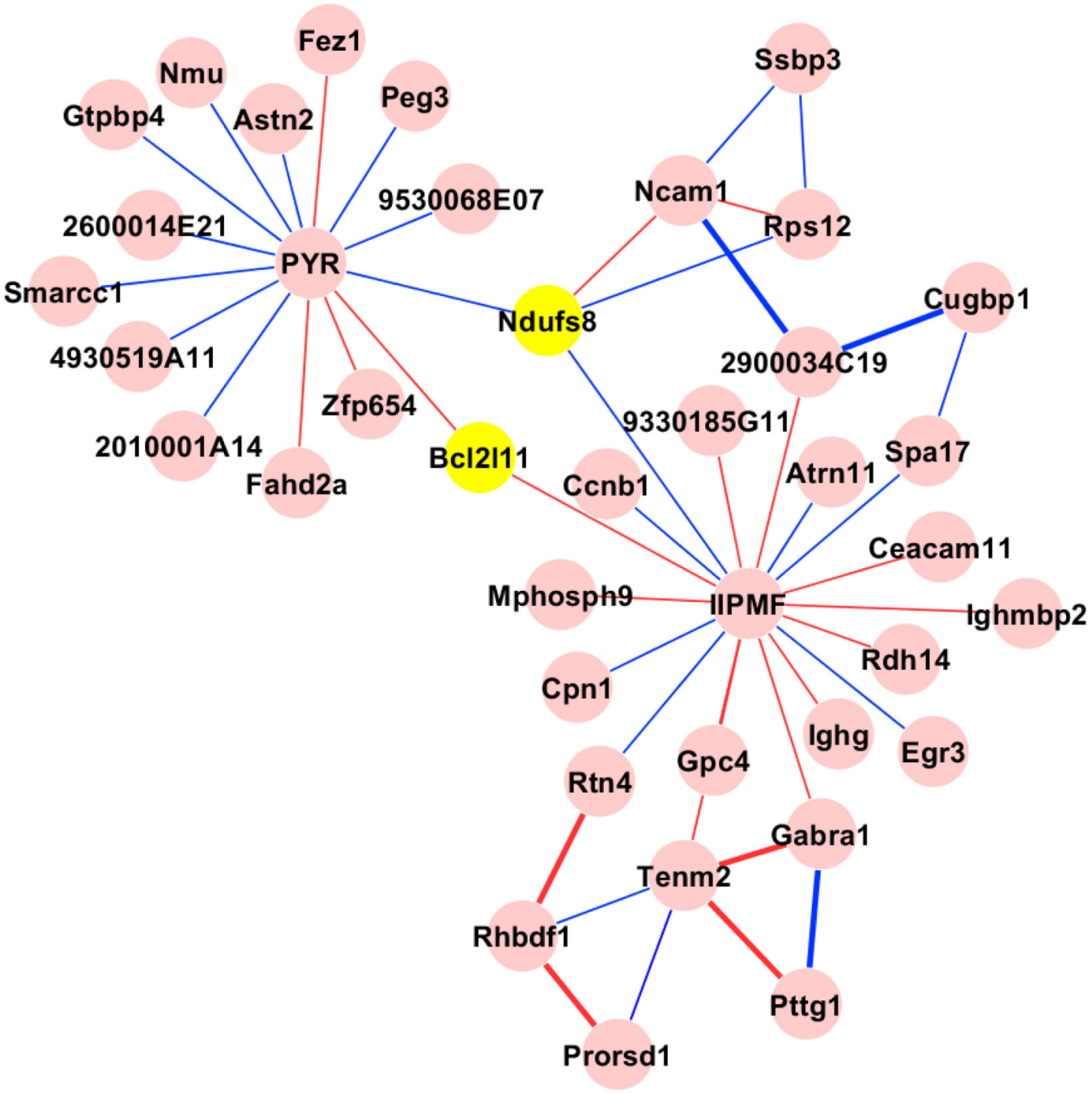

Figure 6. Hippocampal mRNAs associated with IIPMF and stratum pyramidale sizes

Merged network graph of the IIPMF and Stratum pyramidale together with their respective top mRNA correlates expressed in the hippocampus. Edges are colored either red or blue to highlight negative and positive covariates. Line thickness shows correlation strength. There are 2 common genes bridging the graphs that may affect IIPMF and Stratum pyramidale sizes, Bcl2l11, which is strongly associated with apoptosis and Nudfs8, which is a subunit of Mitochondrial complex 1.

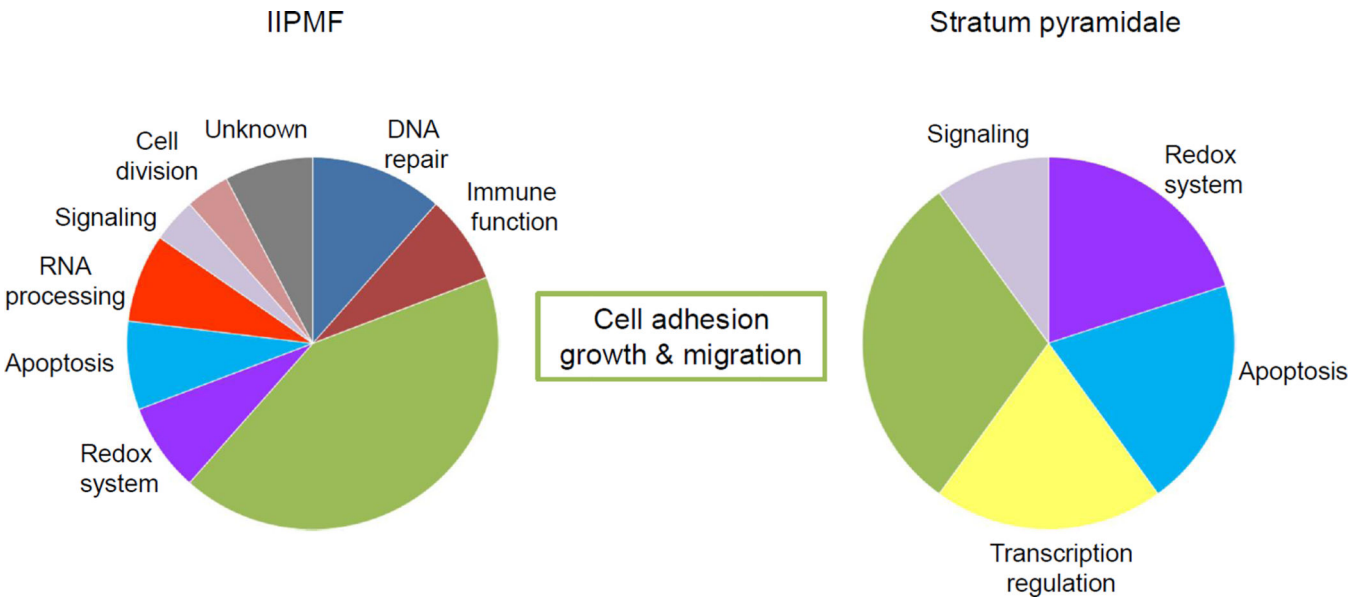

Figure 7. Molecular function enrichment for the IIPMF and stratum pyramidale

Functional assignment of the mRNA covariates affecting IIPMF and stratum pyramidale sizes shows strong themes in cell adhesion, growth, and migration.

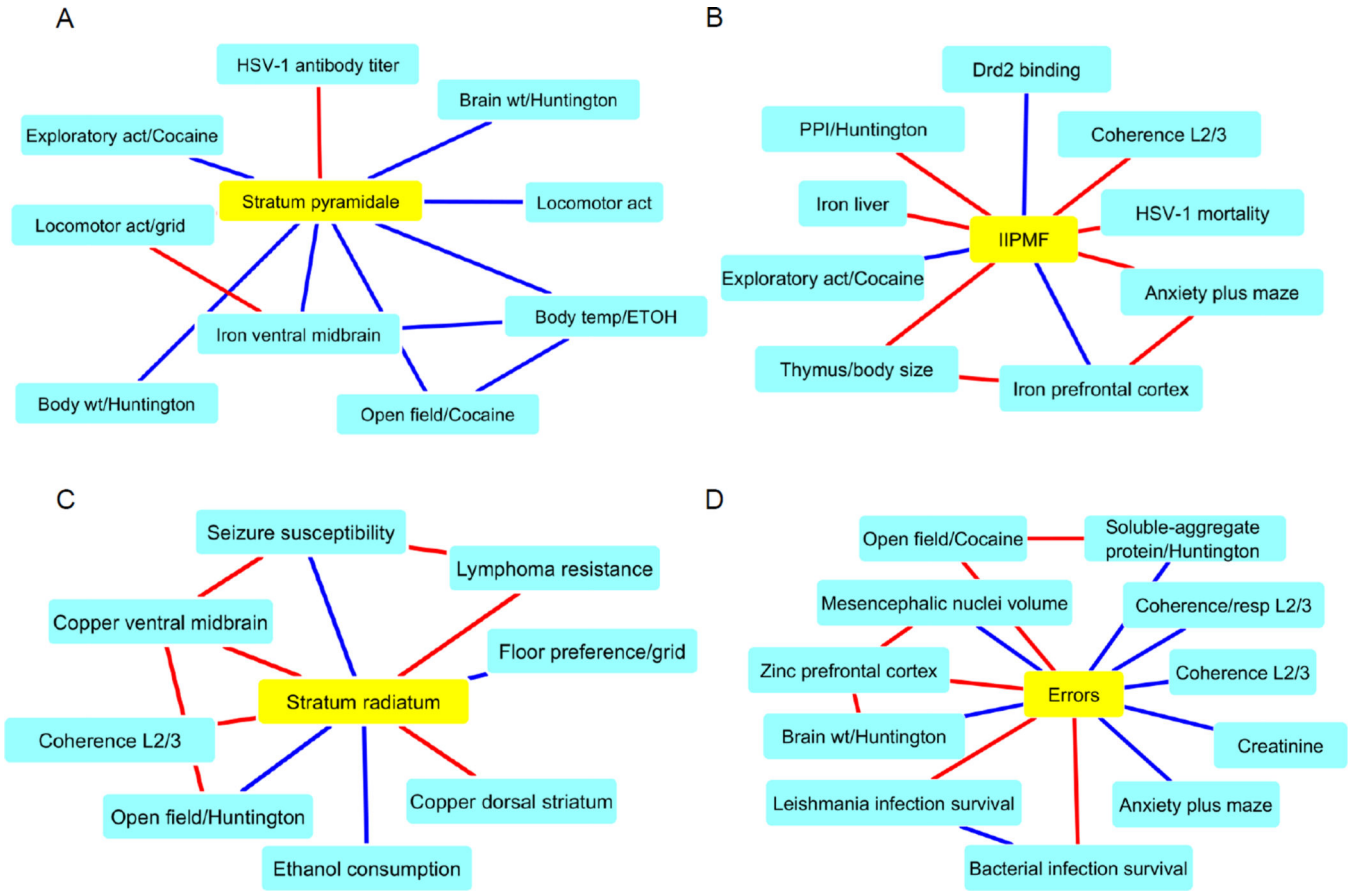

Figure 8. Covariation with traits from the GeneNetwork database

Network diagrams showing covariation among the Stratum pyramidale (A), IIPMF (B), and stratum radiatum (C) sizes and errors in the radial maze test (D) with morphological, behavioral, and physiological phenotypes from the GeneNetwork database. Edges are colored red and blue to highlight negative and positive covariates. Line thickness shows correlation strength. IIPMF data from Lassalle et al. are omitted because of their very high correlation.

Table 1

Significant QTLs for hippocampal morphometry and radial maze learning.

Trait description	LRS	p-value	Chr@Mb
IIPMF (males)	18.241	0.029	X@48.1
Stratum radiatum (males)	17.181	0.043	2@16.2–17.8
Stratum pyramidale (females)	23.389	0.035	11@47.9–50.2
Total errors (females)	17.896	0.035	3@12.6–15.8

Chr@Mb = Chromosome number and Megabase location of QTLs
LRS = liklihood ratio statistic